NASA MEMO 2-18-59W

NASA

MEMORANDUM

THE INTERACTION OF AN OBLIQUE SHOCK WAVE WITH A LAMINAR BOUNDARY LAYER

By R. J. Hakkinen, I. Greber, L. Trilling,
and S. S. Abarbanel

Massachusetts Institute of Technology

NATIONAL AERONAUTICS AND
SPACE ADMINISTRATION

WASHINGTON

March 1959

NATIONAL AERONAUTICS AND SPACE ADMINISTRATION

MEMORANDUM 2-18-59W

THE INTERACTION OF AN OBLIQUE SHOCK WAVE WITH A LAMINAR BOUNDARY LAYER

By R. J. Hakkinen, I. Greber, L. Trilling,
and S. S. Abarbanel

SUMMARY

The results of some experimental and theoretical studies of the interaction of oblique shock waves with laminar boundary layers are presented. Detailed measurements of pressure distribution, shear distribution, and velocity profiles were made during the interaction of oblique shock waves with laminar boundary layers on a flat plate. From these measurements a model was derived to predict the pressure levels characteristic of separation and the length of the separated region.

INTRODUCTION

The interaction of shock waves with boundary layers has been the subject of many recent investigations, both theoretical and experimental. The theoretical predictions of the whole interaction pattern have, in general, been successful only for very weak shocks. The more practical problem of strong shocks has remained largely experimental.

No attempt is made herein to review the many analyses of weak interactions. (See, e.g., refs. 1 and 2.) These analyses generally involve linearized equations of motion, with or without viscous terms, for a flow slightly perturbed from the Blasius flow.

Another semianalytical approach has been to assume that the boundary layer follows a certain pattern and that certain overall parameters are sufficient to characterize it throughout the interaction region. To this class belong the Pohlhausen procedure of Lees (ref. 3) and the integral treatment of Crocco and Lees (ref. 4). A basic assumption of this approach is that there is no pressure gradient across the boundary layer. This is a reasonable condition everywhere except near the shock impingement point and a very useful one because it relates a part of the interaction problem to general boundary-layer theory. (This assumption is used throughout the analyses in the present work.) However, as Gadd points out (ref. 5), any specific velocity profiles chosen may seriously

limit the validity of the analysis in separated flow, and detailed experiments are needed to guide the selection of the analytical model.

The theoretical problem has been eased somewhat by the discovery that the flow parameters near separation depend only on local conditions when the separated region induced by the shock wave is long enough, as has been noted in several researches (e.g., refs. 5 and 6). This forms a basis for the analysis of the present measurements and for the derivation of an analytical model.

The experimental part of this work consisted of measurements of pressure and shear distributions and velocity profiles during shock-wave—boundary-layer interaction on a flat plate. These measurements confirmed that flow parameters near separation are similar. On the basis of the observed flow patterns and simple momentum considerations, estimates were made of the pressure levels near separation; agreement with experiment is good.

Considerations of conservation of mass and momentum led to a law for the variation of length of the separated region with shock strength, Mach number, and Reynolds number. The present measurements verify the dependence on shock strength, but more experiments are needed to check the Mach number and Reynolds number dependence.

This investigation was carried out at the Massachusetts Institute of Technology under the sponsorship and with the financial assistance of the National Advisory Committee for Aeronautics.

SYMBOLS

C Chapman-Rubesin constant defined by $\frac{\mu}{\mu_\infty} = C \frac{T}{T_\infty}$

C_p pressure coefficient, $\frac{p - p_o}{q_o}$

c_f skin-friction coefficient, $\frac{\tau}{q_o}$

F modified Polhausen-Gruschwitz parameter defined in figure 11

H boundary-layer shape factor, $\frac{\delta^*}{\theta}$

h height that line $u = 0$ lies above wall

K Pohlhausen-Gruschwitz parameter

l length of constant-pressure separated region

M Mach number

p pressure

q dynamic pressure, $\frac{1}{2}\rho_o u_o^2$

R_x Reynolds number based on distance from leading edge

R_y Reynolds number based on distance from wall

r recovery factor

T temperature

u component of velocity parallel to plate

v component of velocity normal to plate

x length parallel to plate measured from leading edge of plate

x_l length from leading edge to end of plateau

y length normal to plate

$\beta = \sqrt{M_o^2 - 1}$

γ specific-heat ratio

δ^* boundary-layer displacement thickness

ϵ height which equivalent undisturbed boundary layer is lifted

θ boundary-layer momentum thickness

μ dynamic viscosity coefficient

ν kinematic viscosity coefficient

ρ density

τ shear stress, $\mu \frac{\partial u}{\partial y}$

Subscripts:

o conditions in undisturbed flow before interaction

∞ conditions at outer "edge" of boundary layer

B conditions corresponding to Blasius solution

c conditions which would occur at constant pressure

d difference between final value and value corresponding to incipient separation

f final conditions after incident and reflected shocks

pl conditions at plateau

r reference

s conditions at separation point

ST conditions at stagnation point

w conditions at wall

EXPERIMENTAL APPARATUS AND TECHNIQUE

Wind Tunnel

The experiments were performed in the 8- by 8-inch continuous-flow supersonic wind tunnel in the Gas Turbine Laboratory of the Massachusetts Institute of Technology. This tunnel has a fixed $M = 2$ nozzle with an upward flow direction. A standard schlieren optical system was available for observing and photographing the flow. The tunnel can be operated at stagnation pressures ranging approximately from 3 to 15 pounds per square inch absolute by using a steam-ejector system for evacuation to subatmospheric levels. However, practical problems in manometer accuracy prevented successful operation at the lowest available pressure levels.

Flat Plate

As shown in figure 1, a full-span sharp-nosed flat plate was installed, approximately on the center line of the test section; details of the plate are shown in figure 2. The plate was polished smooth after machining in order to avoid any disturbances which could cause transition of the laminar boundary layer. Forty-five static-pressure orifices were drilled in the plate (using a No. 80 drill) and connected to both mercury and Meriam fluid (specific gravity, 2.95) manometers. The orifices to measure streamwise distribution of static pressure are spaced one-tenth of an inch apart. A thermocouple was installed in the plate surface; its temperature was read by means of a standard potentiometer. Stagnation pressure and temperature were observed similarly, with orifice and thermocouple installed in the settling chamber.

Shock Generator

The adjustable-angle shock generators developed by Barry, Shapiro, and Neumann (ref. 7) for the tunnel were used without changes.

Velocity-Profile and Skin-Friction Measurement

The total head in the boundary layer was measured by a small slit-mouth tube (fig. 3) which could be traversed streamwise and normal to the plate by controls outside the tunnel. The tube height is about 0.004 inch and the opening is about 0.001 inch. The tube location was observed through a cathetometer which was accurate well within 0.001 inch. The velocity profiles were computed in the standard manner assuming constant pressure and total temperature across the boundary layer. This method is believed to be sufficiently accurate except in the immediate neighborhood of the impinging shock.

The same tube was used to measure local skin friction by taking measurements with the tube resting on the plate. A calibration of the tube as a skin-friction meter was made by comparing the tube readings with the measurements of an absolute floating-element skin-friction meter built specifically for this purpose (fig. 4). The theory for the use of small impact pressure probes as skin-friction meters is given in reference 8, in which it is predicted that the difference between the impact pressure measured by the probe resting on the surface and the undisturbed local static pressure is proportional to the 5/3 power of the local shear stress, unless the tube is very small or very large. The calibration of the tube used in the present work was reported in reference 9 and is reproduced in figure 5. It is evident that the

5/3-power law is satisfied and no appreciable compressibility effects are observed.

This calibration was used in the evaluation of the shear-stress distributions in the shock-wave—boundary-layer interaction regions where pressure gradients exist, although the calibration was made with no pressure gradient. (Because of side forces acting on the floating element, it furnishes a reliable reference measurement only under zero pressure gradient.) Because of the small disturbance region of the probe it is believed that the shear-stress measurements are reasonably accurate except perhaps where the pressure gradient is very steep.

Observation of Separation

The location of separation was taken to be the point where the surface skin friction, as measured by the total-head tube resting on the surface of the plate, is zero. Since the instrument was not able to indicate reliable values of negative shear, it was often necessary to extrapolate the zero position from readings of positive skin friction upstream. Although this procedure does not lead to a serious error in the location of separation, it can lead to appreciable error in the determination of the pressure at separation because the pressure gradient near separation is large. This is probably the major cause of scatter in the determination of separation pressure.

In measurements of the minimum shock strength needed to cause separation, the shock generator was adjusted to provide zero skin friction at one point.

Range of Measurements

The experiments were performed at several different shock strengths up to a static-pressure ratio of 2.4, and at different stagnation-pressure (i.e., Reynolds number) levels. The shock strengths ranged from those small enough not to cause separation to cases involving extended upstream influence. The stagnation-pressure range corresponded to Reynolds numbers based on distance from leading edge to shock interaction of 1 to 6×10^5.

Because of the nature of the pressure-level control of the wind tunnel, it was not feasible to attempt to take the measurements following a rigidly specified parameter-variation scheme. It is believed, however, that the results obtained give a reasonable representation of the flow patterns and their characteristics within the overall range of Reynolds numbers and shock strengths.

TYPICAL MEASUREMENTS ON FLAT PLATE

In figure 6 are shown typical pressure distributions, shear distributions, and velocity profiles on the flat plate. Figure 6(a) shows measurements for a shock not sufficiently strong to cause separation. It is seen that the skin-friction coefficient is near the theoretical value[1] upstream of the shock impingement point, falls rapidly to a low value near the shock, then again approaches the theoretical value downstream of the shock. Figure 6(b) shows measurements for a case in which a separated flow region exists. Again the skin-friction coefficient is near the theoretical value both upstream of separation and downstream of reattachment. The velocity profiles indicate that in the separated region the profile above the reverse flow is essentially the undisturbed constant-pressure boundary-layer profile. This will be made a crucial part of the subsequent analysis. The pressure distribution shows a constant-pressure undisturbed region, a pressure rise to a separation, an additional pressure rise beyond separation culminating in a constant-pressure separated region, a pressure rise up to reattachment, and a further pressure rise beyond reattachment culminating in a constant-pressure region corresponding to the pressure downstream of the incident and reflected shocks. Figure 6(c) also shows measurements for a case involving separation. The qualitative picture of the approach to separation and the separated region is similar to that shown in figure 6(b). Shortly after reattachment, however, the skin-friction measurements and the boundary-layer profiles show that the boundary layer becomes turbulent.

Figure 7 shows boundary-layer profiles in the separated region. They indicate that the profile above the reverse flow is essentially an undisturbed boundary-layer profile.

Measurements of pressure distributions, shear distributions, and velocity profiles, similar to the sample ones given in figure 6 are shown in figure 8.

SIMILARITY OF SEPARATION PROPERTIES

Figure 9 is a sketch of typical pressure and shear distributions which occur when a separated region exists and the boundary layer remains

---

[1]The theoretical skin-friction coefficient is calculated from $c_f = c_{f_B}\sqrt{C}$, where c_{f_B} is the Blasius value and C is the Chapman-Rubesin constant defined by $\frac{\mu}{\mu_\infty} = C\,\frac{T}{T_\infty}$. For the conditions of these experiments $C \approx 0.92$.

laminar throughout the interaction region. It is the physical model for the following analysis and defines the quantities which will be used.

Chapman, Kuehn, and Larson (ref. 6) and Gadd (refs. 5 and 10) have pointed out that, at least when there is an appreciable length of separated flow, conditions near separation are independent of the agency which induced separation and the separation phenomenon is essentially similar; all significant parameters are then functions of Mach number and Reynolds number. Thus, the analysis of the shock-wave—boundary-layer interaction can be broken up into two parts: (1) The determination of similar separation properties, which are functions only of local conditions, and (2) the relationship between the length of separated region and the shock strength.

The important parameters involved in separation are the pressure rise to the separation point and the pressure rise to the constant-pressure separated region (henceforth called the "plateau" pressure rise). The minimum pressure rise to cause separation also will be analyzed from the point of view of a similar interaction. Chapman, Kuehn, and Larson have given an order of magnitude analysis which suggests that

$$\Delta C_p \approx \sqrt{\frac{c_{f_o}}{\beta}} \tag{1}$$

In the analysis of Chapman, Kuehn, and Larson the skin-friction coefficient at the beginning of the separating region c_{f_o} is taken as a characteristic skin-friction coefficient for the region, and ΔC_p is a characteristic pressure-rise coefficient for the separating region. Thus, equation (1) should hold both at separation and at the plateau. Gadd's quantitative calculation (ref. 10) also leads to equation (1) for the separation pressure coefficient and determines the constant of proportionality for separation.

Pressure Rise to Separation

The same law (eq. (1)) for the pressure rise to separation, with an estimate of the constant of proportionality, can be obtained from simple momentum considerations, using the observation already made that the undisturbed boundary layer appears to be "lifted" from the wall. Thus, it is assumed that in the approach to separation the boundary layer consists of an outer portion, which differs but little from the undisturbed layer, and a sublayer having small momentum. A sketch of

a typical profile in this region is shown as follows:

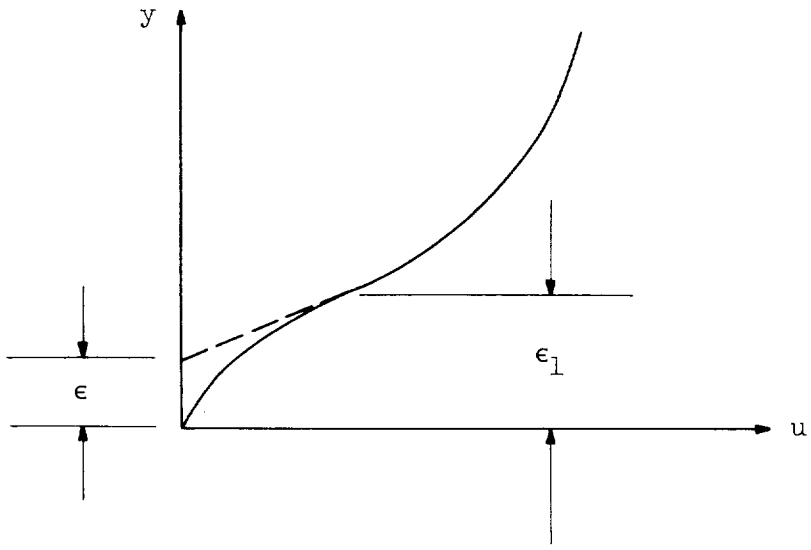

The sublayer joins the outer profile at a height ϵ_1 and, relative to the outer flow, the undisturbed boundary layer appears to be lifted a height ϵ from the wall. If it is assumed that the sublayer has negligible momentum, then the force balance in a region of height ϵ gives

$$\epsilon \frac{dp}{dx} = \tau_\epsilon - \tau_w \tag{2}$$

If the pressure rise is taken to be due to the growth of ϵ and small perturbations are assumed, the pressure rise is related to the rate of growth of the sublayer by

$$C_p = \frac{2}{\beta} \frac{d\epsilon}{dx} \tag{3}$$

Eliminating ϵ between equations (2) and (3) leads to

$$\frac{\beta}{2} \frac{dC_p}{dx} \int_{x_o}^{x} C_p \, dx = c_{f_\epsilon} - c_{f_w} \tag{4}$$

An integration by parts gives

$$\frac{dC_p}{dx}\int_{x_o}^{x} C_p\,dx = \frac{C_p^2}{2} + \int_{x_o}^{x} C_p''(\xi)\left[\int_{\xi_o}^{\xi} C_p(\eta)\,d\eta\right]d\xi \tag{5}$$

Since up to the point of separation C_p'' is small except for a small region in which C_p is small, the integral on the right-hand side of equation (5) is small in comparison with C_p^2. Neglecting this integral and evaluating equation (4) at the separation point where $c_{f_w} = 0$ gives the separation pressure rise as

$$C_{p_s} = 2\sqrt{\frac{\left(c_{f_\epsilon}\right)_s}{\beta}} \tag{6}$$

where $\left(c_{f_\epsilon}\right)_s$ is the skin-friction coefficient at ϵ at the separation point.

To evaluate $\left(c_{f_\epsilon}\right)_s$ the form of the sublayer profile must be chosen. Equation (2) implies that the parabolic profile which must exist at the wall adequately describes the profile for a small distance away from the wall. Thus, an integration of the wall condition

$$\frac{dp}{dx} = \left(\frac{\partial \tau}{\partial y}\right)_w \tag{7}$$

leads to the profile

$$u = \frac{\tau_w}{\mu_w}\,y + \frac{dp/dx}{2\mu_w}\,y^2 \tag{8}$$

The parabolic profile and the "undisturbed" profile are joined at ϵ_1, the matching conditions being

$$u(\epsilon_1) = \frac{\tau_w}{\mu_w}\epsilon_1 + \frac{dp/dx}{2\mu_w}\epsilon_1^2 \tag{9}$$

$$u(\epsilon_1) = \frac{\tau_o}{\mu_w}(\epsilon_1 - \epsilon) \tag{10}$$

$$\tau(\epsilon_1) = \tau_o = \tau_w + \frac{dp}{dx}\epsilon_1 \tag{11}$$

Actually $\tau(\epsilon_1)$ must be a little less than τ_o because there is an adjustment region before the region of fairly constant pressure gradient is reached. This adjustment region is ignored. Solving equations (9), (10), and (11) for ϵ gives

$$\epsilon = \frac{\tau_o}{2\frac{dp}{dx}}\left(1 - \frac{\tau_w}{\tau_o}\right)^2 \tag{12}$$

At the separation point $\tau_w = 0$ and it is found that $\tau_\epsilon = \frac{1}{2}\tau_o$. Thus, the separation pressure coefficient is

$$C_{p_s} = \sqrt{\frac{2c_{f_o}}{\beta}} \tag{13}$$

In figure 10 are shown the separation pressure rises measured in the present work. Within the scatter of the experimental points it is seen that equation (13) correlates the data reasonably well. As previously pointed out, the large scatter is due primarily to the fact that small errors in the location of the separation point lead to large errors in the separation pressure because of the large pressure gradient near

separation. For additional comparison, Gadd's theory (ref. 10) gives $C_{p_s} = 1.39\sqrt{\frac{c_{f_o}}{\beta}}$, in agreement with the result of the simple reasoning just given. The data correlated by Chapman, Kuehn, and Larson show a slightly lower value; from these data, at $M_o = 2$, $C_{p_s} = 1.19\sqrt{\frac{c_{f_o}}{\beta}}$.

It is interesting to examine the effect of employing the same basic assumptions within the framework of the Kármán integral equation of boundary-layer momentum. For small disturbances from free-stream conditions this equation can be written

$$c_f = 2\frac{d\theta}{dx} - \left[\delta^* + \theta\left(2 - M_o^2\right)\right]\frac{dC_p}{dx} \tag{14}$$

Corresponding to the assumption that the boundary layer is lifted by a sublayer of negligible momentum, the momentum thickness can be approximated by its constant-pressure value. Writing the displacement thickness as the constant-pressure value plus a deviation from it and writing instead of equation (3)

$$C_p = \frac{2}{\beta}\frac{d(\Delta\delta^*)}{dx} \tag{15}$$

where $\Delta\delta^*$ is the deviation from the constant-pressure displacement thickness, gives on substitution into equation (14) the following equation:

$$c_{f_c} - c_{f_w} = \left(H_c + 2 - M_o^2\right)\theta_c\frac{dC_p}{dx} + \frac{\beta}{2}\frac{dC_p}{dx}\int_{x_o}^{x} C_p\,dx \tag{16}$$

where the subscript c denotes the constant-pressure value. As before, an integration by parts is performed and then an evaluation of equation (16) at the separation point, where $c_{f_w} = 0$, gives

$$\frac{\beta}{4} C_{p_s}{}^2 = \left(c_{f_c}\right)_s - \left(H_c + 2 - M_o{}^2\right)\left(\theta_c \frac{dC_p}{dx}\right)_s \tag{17}$$

Now, if the boundary-layer separation mechanism simply involves the action of an adverse pressure gradient, then perhaps an estimate of $\left(\theta_c \frac{dC_p}{dx}\right)_s$ can be obtained from the extended Pohlhausen calculation (e.g., ref. 11). The boundary layer is then described by the Pohlhausen-Gruschwitz parameter K, which at separation can be written

$$K_s = -\left(\frac{\rho_\infty}{\rho_w} \frac{\theta^2}{C} \frac{u_\infty}{2\nu_\infty} \frac{dC_p}{dx}\right)_s = -0.157 \tag{18}$$

Equation (18) leads to the approximate result

$$\left(\theta \frac{dC_p}{dx}\right)_s = \frac{0.713\left(c_{f_c}\right)_s}{1 + \frac{\gamma - 1}{2} r M_o{}^2} \tag{19}$$

or, since $\theta_c = x c_{f_c}$,

$$\left(x \frac{dC_p}{dx}\right)_s = \frac{0.713}{1 + \frac{\gamma - 1}{2} r M_o{}^2} \tag{20}$$

Note that although equations (19) and (20) have the form of the incompressible equations, they actually are valid for compressible flow because of the use of the Chapman-Rubesin constant C.

In equations (19) and (20) r is the recovery factor. Equation (20) is subject to experimental verification. Data from the NACA, the University of Southern California, the Massachusetts Institute of Technology, and the National Physical Laboratory for a Mach number range of 2.0 to 2.53 and a

Reynolds number range of 76,000 to 1,130,000 in which separation was induced by a step, a corner, and a reflecting shock wave are plotted in figure 11. Considering the difficulty in measuring an experimental pressure gradient, these data do indicate that the product $x \frac{dC_p}{dx}$ at separation is constant at a given Mach number but that the constant is less than half the Pohlhausen-Gruschwitz constant. Adjusting the constant and putting equation (19) into equation (17) give the following equation for the separation pressure coefficient:

$$C_{p_s} = 2\sqrt{\frac{\left(c_{f_c}\right)_s}{\beta}}\sqrt{1 - \frac{0.3\left(H_c + 1 - M_o^2\right)}{1 + \frac{\gamma - 1}{2} r M_o^2}} \tag{21}$$

From the work of Chapman and Rubesin (ref. 12), the following equation can be derived for $\gamma = 1.4$ and Prandtl number = 0.72:

$$H_c = H_B\left(1 + 0.258M_o^2\right) \tag{22}$$

The subscript B denotes the Blasius value. Therefore, for $M_o = 2$, equation (21) shows that

$$C_{p_s} = 1.29\sqrt{\frac{\left(c_{f_c}\right)_s}{\beta}} \tag{23}$$

The reasonable agreement between equations (13) and (23) indicates that the integral momentum equation may be satisfactory even in strong pressure gradients in supersonic flow if it is applied judiciously. The failure of the Pohlhausen-Gruschwitz parameter to describe the pressure gradient at separation is due to the inadequate representation of the boundary-layer profile; the integral equation is not at all involved in this calculation.

It is expected that the correction to the Pohlhausen-Gruschwitz parameter depends upon the Mach number. Lacking an extension of the correction to Mach numbers other than 2, the simpler equation (13)

should be used at other Mach numbers. The agreement between equations (13) and (23) will be taken as justification for reasoning from the integral momentum equation.

Pressure Rise to Plateau

Beyond the separation point the analysis is more difficult. Clearly, the parabolic approximation for the inner boundary-layer profile cannot hold throughout this region both because it would degenerate to an incorrect linear one when the plateau is reached and because the inertia forces, far from being negligible, must balance the shear forces when the plateau is reached. However, it is expected that the inertia forces and the curvature of the pressure distribution will come into play about the same time; since they are of the same order and make contributions of opposite sign, an order of magnitude can be estimated by neglecting both of them. With this approach

$$C_{p_{pl}}{}^2 \approx \frac{4}{\beta}\left(c_{f_\epsilon} - c_{f_w}\right)_{pl} \tag{24}$$

This is then really the same as the condition prior to separation. Now, c_{f_ϵ} must be less than the maximum value of c_f anywhere in the profile at the beginning of the plateau, and the profiles show that this maximum is less than, say, $0.9c_{f_o}$. If a symmetrical backflow is assumed at the plateau, the following approximate upper limit is obtained for the plateau pressure:

$$C_{p_{pl}} < 1.9\sqrt{\frac{2c_{f_o}}{\beta}} \tag{25}$$

or

$$C_{p_{pl}} < 1.9C_{p_s} \tag{26}$$

Another estimate of order of magnitude can be made by adopting the point of view that beyond separation the line $u = 0$ forms a wall around which the boundary layer is deflected. Then the integral momentum equation (14) can be applied above $u = 0$. If the line $u = 0$ is lifted

a height h from the wall, then the following equation analogous to equation (16) is obtained:

$$c_{f_c} - c_{f_h} = \left(H_c + 2 - M_o^2\right)\theta_c \frac{dC_p}{dx} + \frac{\beta}{2}\frac{dC_p}{dx}\int_{x_o}^{x} C_p\,dx - \frac{dC_p}{dx}\int_{x_s}^{x}\frac{dh}{dx}\,dx \tag{27}$$

Now the pressure distribution in the vicinity of the separation point has the following qualitative form:

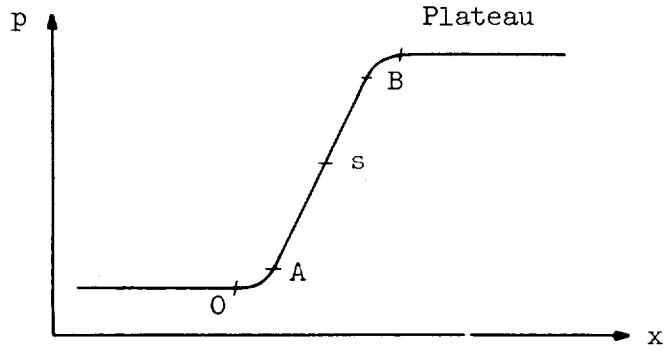

At the beginning of the interaction region, between points 0 and A, there is a decrease of wall shear and an increase of pressure gradient which occurs with negligible pressure rise until the pressure gradient approaches the separation value. Between points A and B the pressure increases at almost constant pressure gradient. Beyond point B there is a decrease in pressure gradient, and the reverse flow momentum goes from a negligible value to its equilibrium value at the plateau.

If most of the pressure rise to the plateau occurs before the reverse flow momentum becomes important (i.e., before point B which would give a lower limit for the plateau pressure), then

$$\frac{dC_p}{dx}\int_{x_s}^{x}\frac{dh}{dx}\,dx = c_{f_h} - c_{f_w} \tag{28}$$

When the plateau is reached the plateau pressure coefficient is due primarily to the angle which the line $u = 0$ makes with the wall, and

3A

the boundary layer above $u = 0$ must have thinned down between the separation point and the plateau so that $d\delta^*/dx$ is again small. It is expected that the decrease in pressure gradient between point B and the plateau is accompanied by an increase of shear stress at $u = 0$ in the same manner as the increase in pressure gradient between points o and A is accompanied by a decrease in wall shear. If it is assumed that the deviation of the skin-friction coefficient at $u = 0$ from the constant-pressure value is the same at points A and B, then if the pressure at point B is identified with that at the plateau and the additional assumption is made that $c_{f_w} \approx -c_{f_h}$ when the plateau is approached, equation (27) leads to

C-474

$$C_{p_{pl}} > C_{p_s}\sqrt{2} \tag{29}$$

Taking the mean between the estimates of equations (26) and (29) as the approximate plateau pressure coefficient gives

$$C_{p_{pl}} = 1.65C_{p_s} \tag{30}$$

Using equation (13) to give C_{p_s} there results

$$C_{p_{pl}} = 1.65\sqrt{\frac{2c_{f_o}}{\beta}} \tag{31}$$

The data plotted in figure 10 show good agreement with the results of equation (31). The correlation of data in reference 6 gives, for $M_o = 2$, $C_{p_{pl}} = 2\sqrt{\frac{c_{f_o}}{\beta}}$, which is about 13 percent lower than the value given by equation (31). On the other hand, the correlation indicates that $C_{p_{pl}}$ is 1.68 times the correlated C_{p_s}, in agreement with equation (30).

In figure 12 is plotted the variation with Mach number of the separation and plateau pressure coefficients as given by equations (13) and (31) and by the correlation of data of reference 6. Also shown is the data of the present work. Considering the scatter of the experimental data it can be concluded that the separation and plateau pressure coefficients are reasonably well predicted by equations (13) and (31).

Pressure Rise for Incipient Separation

For shock strengths just great enough to create zero wall friction at one point, the observed flow pattern is as shown in figure 13. In the vicinity of the shock the pressure gradient on the surface is maintained reasonably constant by the external shock configuration, although the self-induced gradient would be negative as the boundary-layer edge becomes convex. It can be argued, however, that the local effect of the shock system cannot extend very far from the impingement point since the pressure jump is progressively canceled by the expansions when the surface is approached. This view seems to be supported by the experiments. Thus, the pressure rise is due primarily to the self-induced effect, and the pressure rise to separation should be about the same as that for separation well upstream of the shock. If symmetry of thickening and thinning of the boundary layer is assumed, there results

$$\left(c_p\right)_{\text{incipient}} = 2c_{p_s} \tag{32}$$

The data shown in figure 10 support rather well this simple point of view.

LENGTH OF SEPARATED REGION

When the flow is completely separated, the height of the separated region depends on the mass of fluid forced into the backflow by the overpressure left available from the main shock after subtracting the sum of the pressure rise from undisturbed conditions to the plateau and the pressure rise associated with the reattachment process. Now, all the fluid which is reversed must come from above the line $u = 0$ as shown by the following sketch:

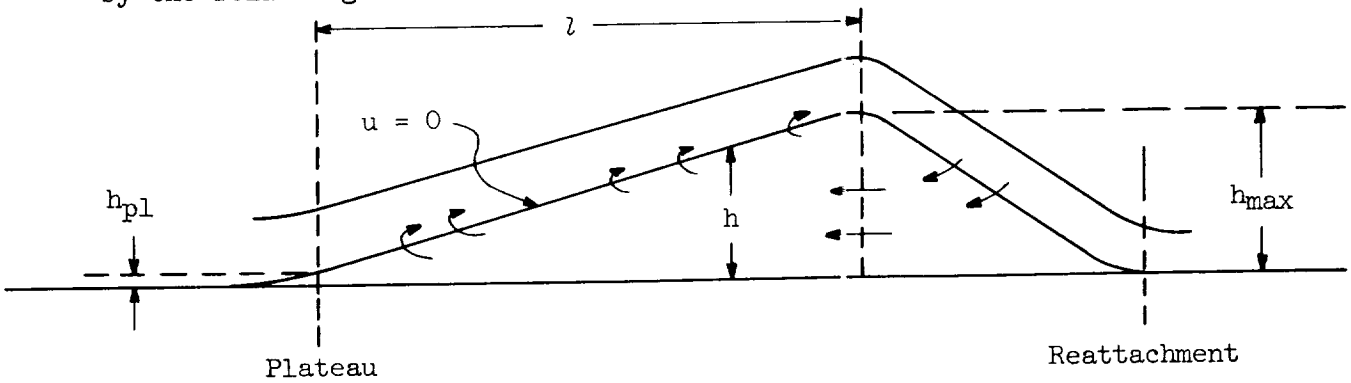

If the boundary-layer equations are used again, the integral of the momentum equation is

$$\int \left(\rho u \frac{\partial u}{\partial x} + \rho v \frac{\partial u}{\partial y} + \frac{dp}{dx} \right) dx = \int \frac{\partial \tau}{\partial y} dx \tag{33}$$

This integral is to be evaluated along the line $u = 0$ from the maximum height of the separated region to the reattachment point. At the beginning of the reattachment process $\frac{\partial \tau}{\partial y}$ must be of order $\rho v_{pl} \left(\frac{\partial u}{\partial y} \right)_{pl}$. In the approach to reattachment $\left| v \right| \gg \left| v_{pl} \right|$ for long plateaus, and the pressure gradient increases rapidly. It is therefore expected that for a while the opposite effects on $\frac{\partial \tau}{\partial y}$ of the adverse pressure gradient and the suction through $u = 0$ would tend to cancel each other, and hence it seems fair to neglect $\int \frac{\partial \tau}{\partial y} dx$. Thus,

$$\Delta p_d \approx - \int \rho v \frac{\partial u}{\partial y} dx \tag{34}$$

where Δp_d is the driving pressure for the reverse flow. Taking averages gives

$$\Delta p_d \approx -\rho_w \bar{v} \frac{\bar{\tau}}{\mu_w} \Delta x \tag{35}$$

By continuity, $-\rho_w \bar{v} \Delta x = \rho_w \bar{u} h_{max}$, and thus equation (35) becomes

$$\Delta p_d \frac{\mu_w}{\bar{\tau}} = \rho_w \bar{u} h_{max} \tag{36}$$

A momentum balance in the separated region at h_{max} gives approximately

$$\rho_w \bar{u}^2 \frac{dh}{dx} = \frac{\beta}{2} \rho_w \bar{u}^2 C_{p_{pl}} = \tau_{u=0} - \tau_w \approx 2\bar{\tau} \tag{37}$$

where the reverse flow has been assumed to be symmetrical.

Eliminating $\bar{u}$ between equations (36) and (37) and writing

$$h_{max} = h_{pl} + \frac{\beta}{2} C_{p_{pl}} l \tag{38}$$

where l is the length of the plateau gives, for a value of h_{pl} which is small in comparison with h_{max},

$$\bar{c}_f^3 q_o \rho_w \beta C_{p_{pl}} l^2 = \mu_w^2 \Delta C_{p_d} \tag{39}$$

Replacing $C_{p_{pl}}$ by its value from equation (38) and letting x_r be any reference length, there results from equation (39)

$$\frac{l}{x_r} = 2.1\left(1 + \frac{\gamma - 1}{2} r M_o^2\right)^{3/2} \beta^{-1/4} c_{f_r}^{2} \bar{c}_f^{-3/2} c_{f_o}^{-1/4} \Delta C_{p_d} \tag{40}$$

where c_{f_r} is the constant-pressure skin-friction coefficient at the reference station x_r. If the reference length x_l is taken as the length from the leading edge to the end of the plateau, then $c_{f_r} = c_{f_{x_l}}$ and

$$c_{f_o} \approx c_{f_{x_l}}\left(1 - \frac{l}{x_l}\right)^{-1/2} \tag{41}$$

In the absence of mixing, $\bar{c}_f \approx c_{f_{x_l}}$. Accepting this value for the moment, equation (40) leads to

$$\frac{l}{x_l}\left(1 - \frac{l}{x_l}\right)^{-1/2} = 2.1\left(1 + \frac{\gamma - 1}{2} r M_o^2\right)^{3/2} \beta^{-1/4} c_{f_{x_l}}^{1/4} \Delta C_{p_d} \qquad (42)$$

The important results of equation (42) are that the length of the separated region depends strongly on the driving pressure and only weakly on the Reynolds number.

The driving pressure is not too easily determined from experiment, and it would be useful if it were not necessary to do so. A plausible choice for the driving pressure is the difference between the final pressure and the pressure for incipient separation. Thus,

$$\Delta C_{p_d} = C_{p_f} - \left(C_p\right)_{\text{incipient}} = C_{p_f} - 2C_{p_s} = C_{p_f} - 1.21C_{p_{pl}} \qquad (43)$$

The last form is the most useful, since C_{p_f} and $C_{p_{pl}}$ are easy to measure and the other quantities are not. With this choice of ΔC_{p_d}, the lengths of the separated regions are plotted in figure 14. The linear relationship between the function of length of the separated region and the driving pressure is clear $\left(c_{f_{x_l}}^{1/4}\right.$ is not a major variable in these tests$\left.\right)$. However, the constant of proportionality is greater than that of equation (42) and the line does not go through the origin. Both of these results are not unexpected. For short lengths of separated region the reverse flow is not well established, the wall shear must be close to zero, and, hence, the effective $\bar{c}_f$ must be much less than the local constant-pressure value. Consequently, for small lengths of separated region the length should grow more rapidly than for larger lengths in which the backflow is well established. The constant of proportionality is larger than that predicted by equation (42) because $\bar{c}_f$ really is somewhat less than $c_{f_{x_l}}$. Using the experimental slope and intercept, equation (42) becomes, for the longer separated regions,

$$\frac{l}{x_l}\left(1 - \frac{l}{x_l}\right)^{-1/8} = 2.53\left(1 + \frac{\gamma - 1}{2} rM_o^2\right)^{3/2} \beta^{-1/4} c_{f_{x_l}}{}^{1/4} \Delta C_{p_d} + 0.097 \qquad (44)$$

The new constant of proportionality implies that $\bar{c}_f \approx 0.82 c_{f_{x_l}}$ which is quite a reasonable figure. Thus, the experiments seem to support the proposed model. More experiments are needed, however, to verify the Mach number and Reynolds number dependence.

CONCLUDING REMARKS

An experimental and theoretical analysis of the interaction between a shock wave and a laminar boundary layer has been made. The qualitative picture of the interaction is as follows:

The adverse pressure gradient due to a shock wave causes the wall shear to decrease upstream of the shock wave. When the pressure rise reaches a certain threshold the wall shear is brought to zero. For larger pressure rises a separated region occurs.

The experiments show, as also is reported in other researches, that when the separated flow region is sufficiently long the pressure levels associated with separation depend only on local conditions. It is observed from the boundary-layer profiles that the profiles are modified primarily near the wall, the outer flow remaining essentially an undisturbed boundary layer. An analysis of the separation pressure levels based on this observation gives reasonable agreement with the measurements. It is also shown that the integral momentum equation can be used to predict the separation pressure levels provided that an adequate measure of the pressure gradient at separation can be made.

An analysis of the length of the separated region shows that it is almost proportional to the pressure rise over and above that needed to induce incipient separation and that it varies only weakly with the Reynolds number; the length is inversely proportional to the eighth root of the Reynolds number. The measurements also support this analysis.

Massachusetts Institute of Technology,
Cambridge, Mass., May 1, 1957.

REFERENCES

1. Lighthill, M. J.: On Boundary Layers and Upstream Influence. II. Supersonic Flows Without Separation. Proc. Roy. Soc. (London), ser. A, vol. 217, 1953, pp. 478-507.

2. Müller, Ernst-August: Theoretische Untersuchungen über die Wechselwirkung zwischen einem einfallenden schwachen Verdichtungsstoss und der laminaren Grenzschict in einer Überschallströmung. 50 Jahre Grenzschichtforschung, Friedr. Viewag & Sohn (Braunschweig), 1955, pp. 343-363.

3. Lees, L.: Interaction Between the Laminar Boundary Layer Over a Plane Surface and an Incident Oblique Shock Wave. Rep. No. 143, Princeton Univ., Aero. Eng. Lab., Jan. 24, 1949.

4. Crocco, Luigi, and Lees, Lester: A Mixing Theory for the Interaction Between Dissipative Flows and Nearly-Isentropic Streams. Jour. Aero. Sci. vol. 19, no. 10, Oct. 1956.

5. Gadd, G. E.: Interactions Between Wholly Laminar or Wholly Turbulent Boundary Layers and Shock Waves Strong Enough To Cause Separation. Jour. Aero. Sci., vol. 20, no. 11, Nov. 1953, pp. 729-739.

6. Chapman, Dean R., Kuehn, Donald M., and Larson, Howard, K.: Investigation of Separated Flows in Supersonic and Subsonic Streams With Emphasis on the Effect of Transition. NACA TN 3869, 1957.

7. Barry, F. W., Shapiro, A. H., and Neumann, E. P.: The Interaction of Shock Waves With Boundary Layers on a Flat Surface. Guided Missiles Program, M.I.T. Meteor Rep. No. 52, Mar. 1950.

8. Trilling, L., and Hakkinen, R. J.: The Calibration of the Stanton Tube as a Skin-Friction Meter. 50 Jahre Grenzschichtforschung, Friedr. Viewag & Sohn (Braunschweig), 1955, pp. 201-209.

9. Abarbanel, S. S.: The Calibration of the Stanton Tube as a Skin Friction Meter. M. S. Thesis, M.I.T., 1955.

10. Gadd, G. E.: A Theoretical Investigation of the Effects of Mach Number, Reynolds Number, Wall Temperature and Surface Curvature on Laminar Separation in Supersonic Flow. Rep. No. FM 2415, British A.R.C., June 1956.

11. Schlichting, Hermann (J. Kestin, trans.): Boundary Layer Theory. McGraw-Hill Book Co., Inc., 1955.

12. Chapman, Dean R., and Rubesin, Morris W.: Temperature and Velocity Profiles in the Compressible Laminar Boundary Layer With Arbitrary Distribution of Surface Temperature. Jour. Aero. Sci., vol. 16, no. 9, Sept. 1949, pp. 547-565.

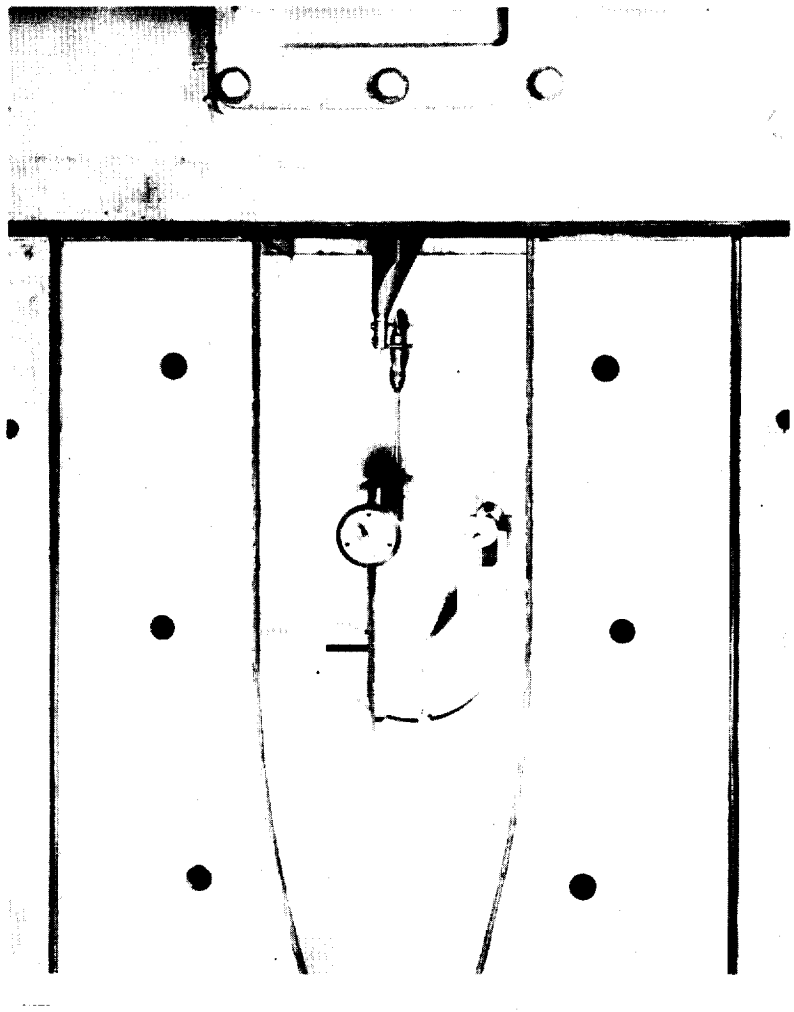

L-58-3795

Figure 1.- Flat plate mounted in wind tunnel.

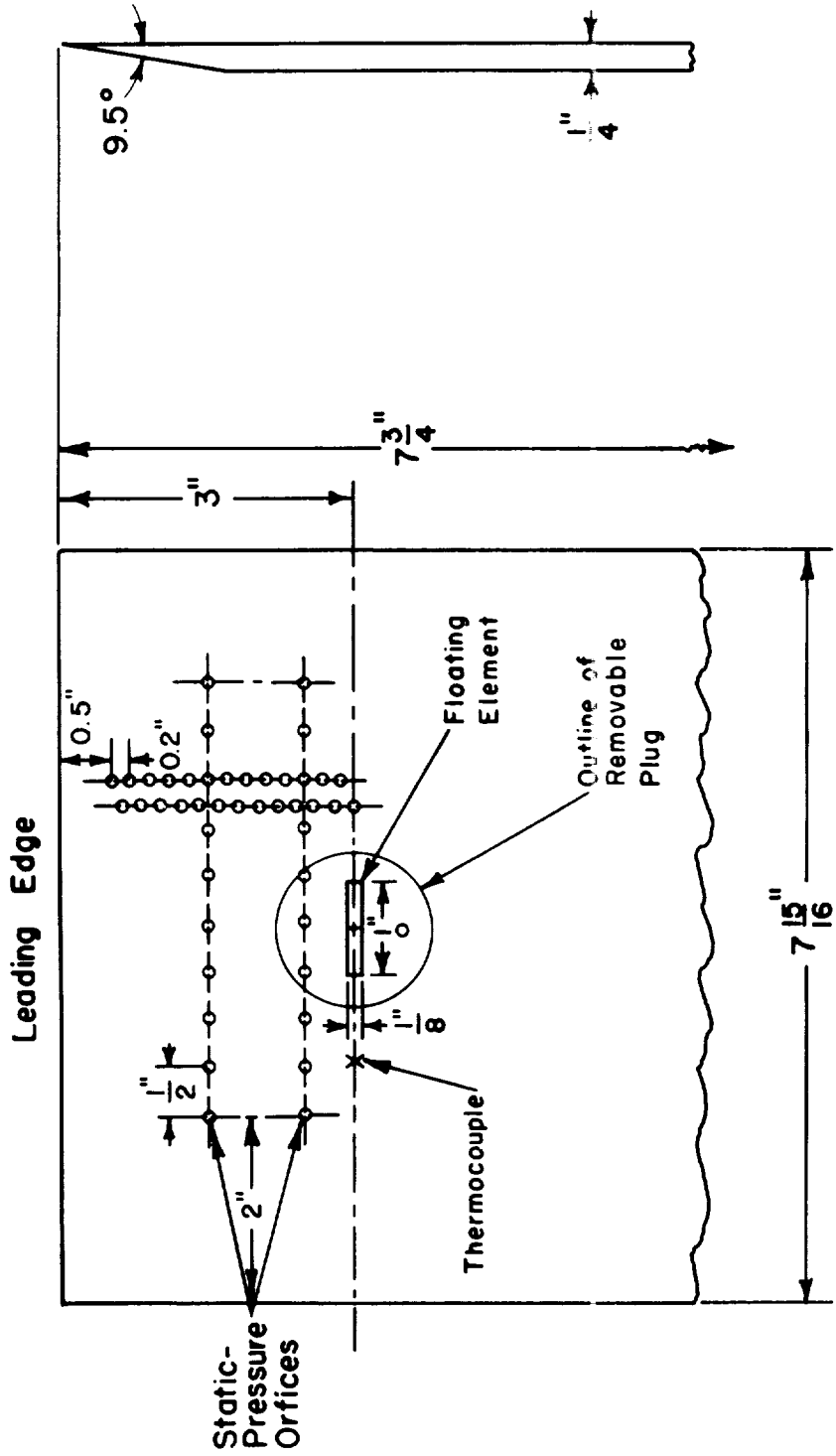

Figure 2.- Details of flat plate.

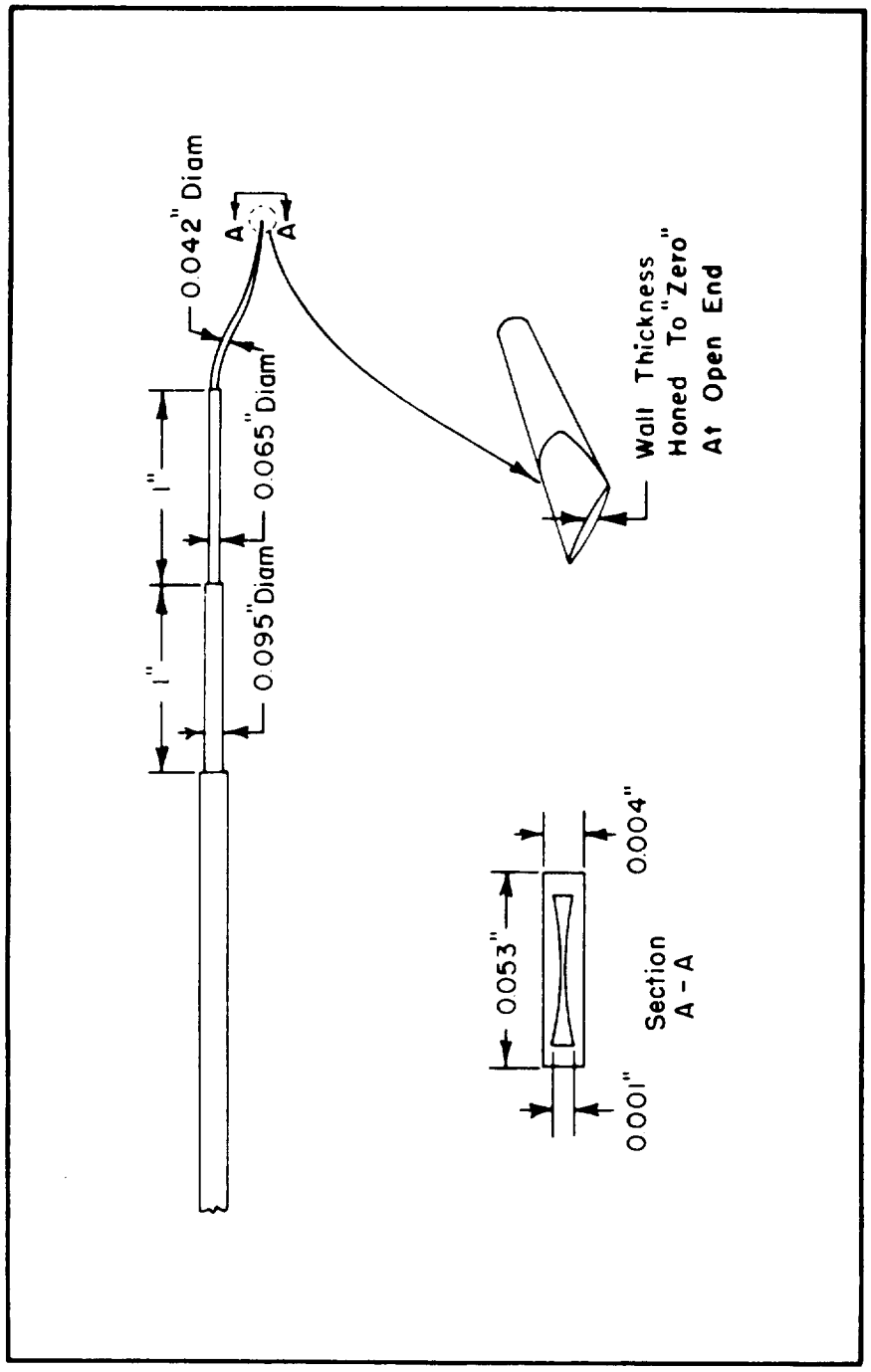

Figure 3.- Stanton tube configuration.

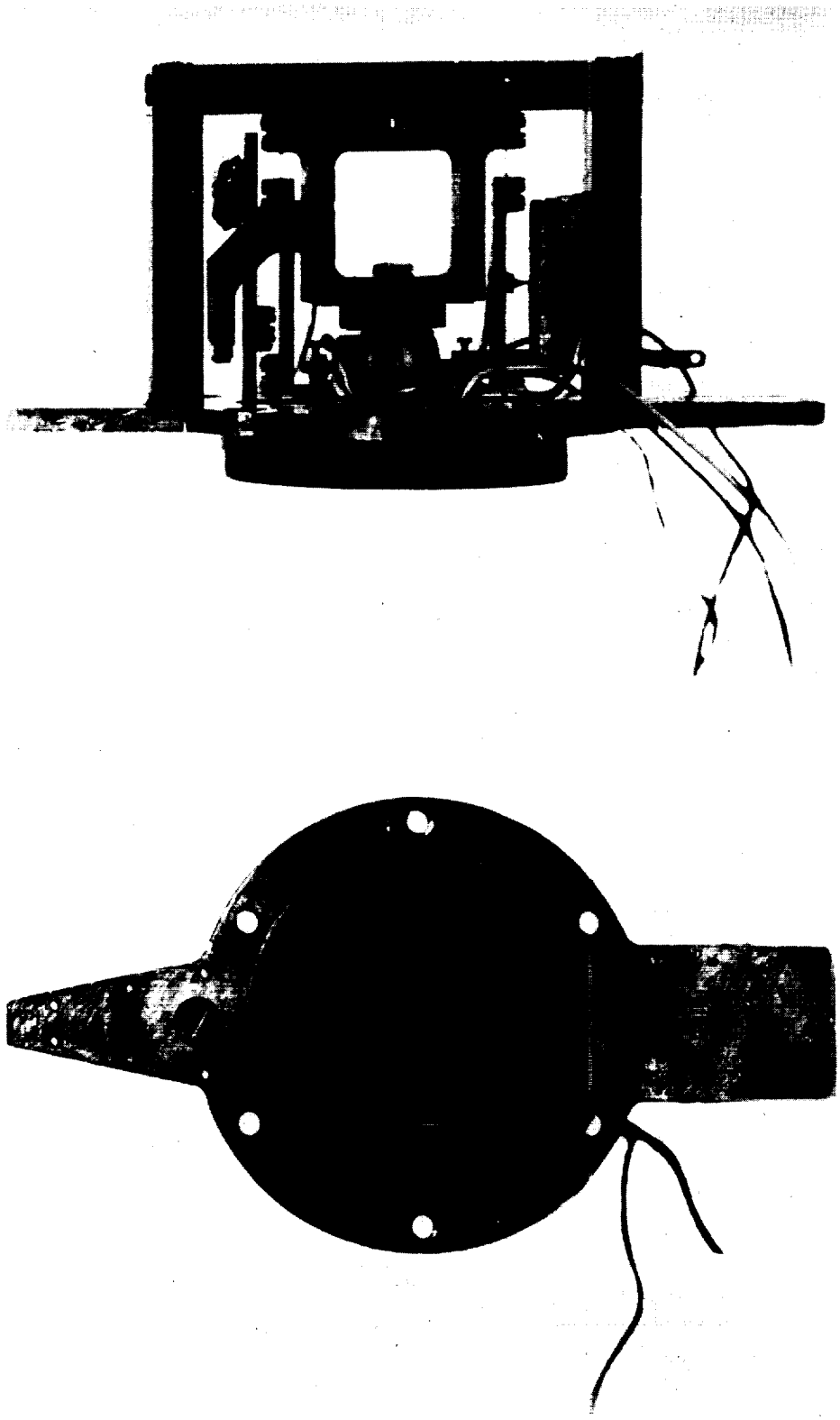

L-58-3796

Figure 4.- Floating-element skin-friction meter.

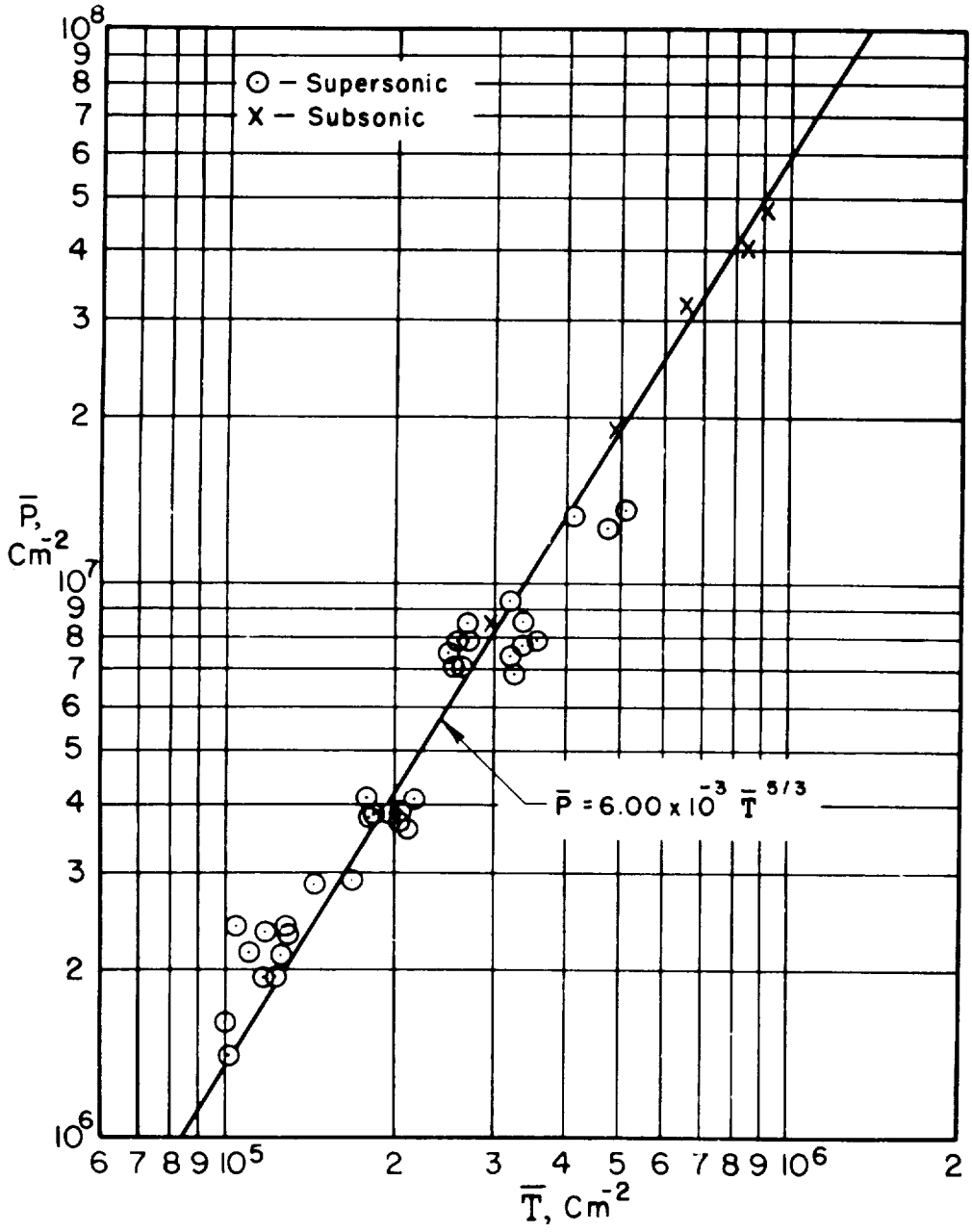

Figure 5.- Stanton tube calibration. $\bar{P} = \frac{(p_{tube} - p_o)\rho_w}{\mu_w^2}$; $\bar{T} = \frac{\tau_w \rho_w}{\mu_w^2}$.

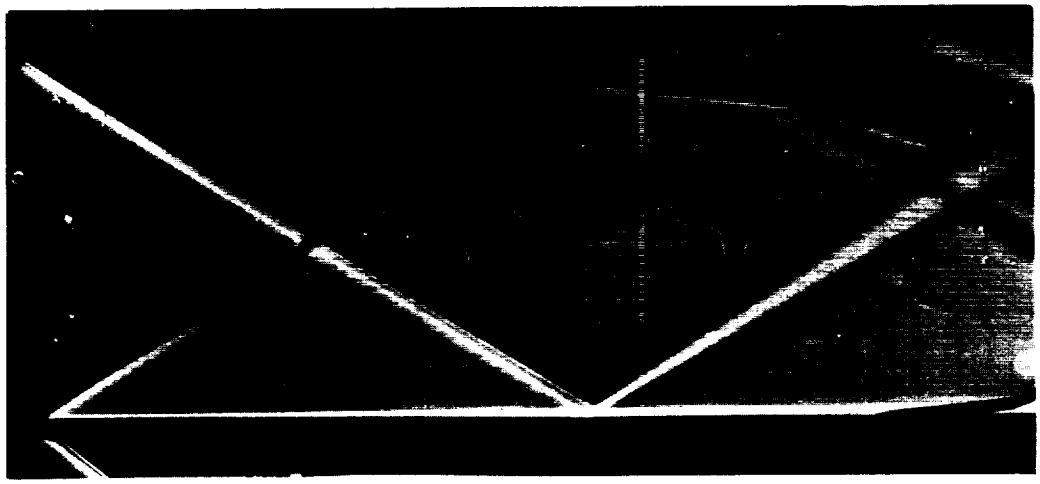

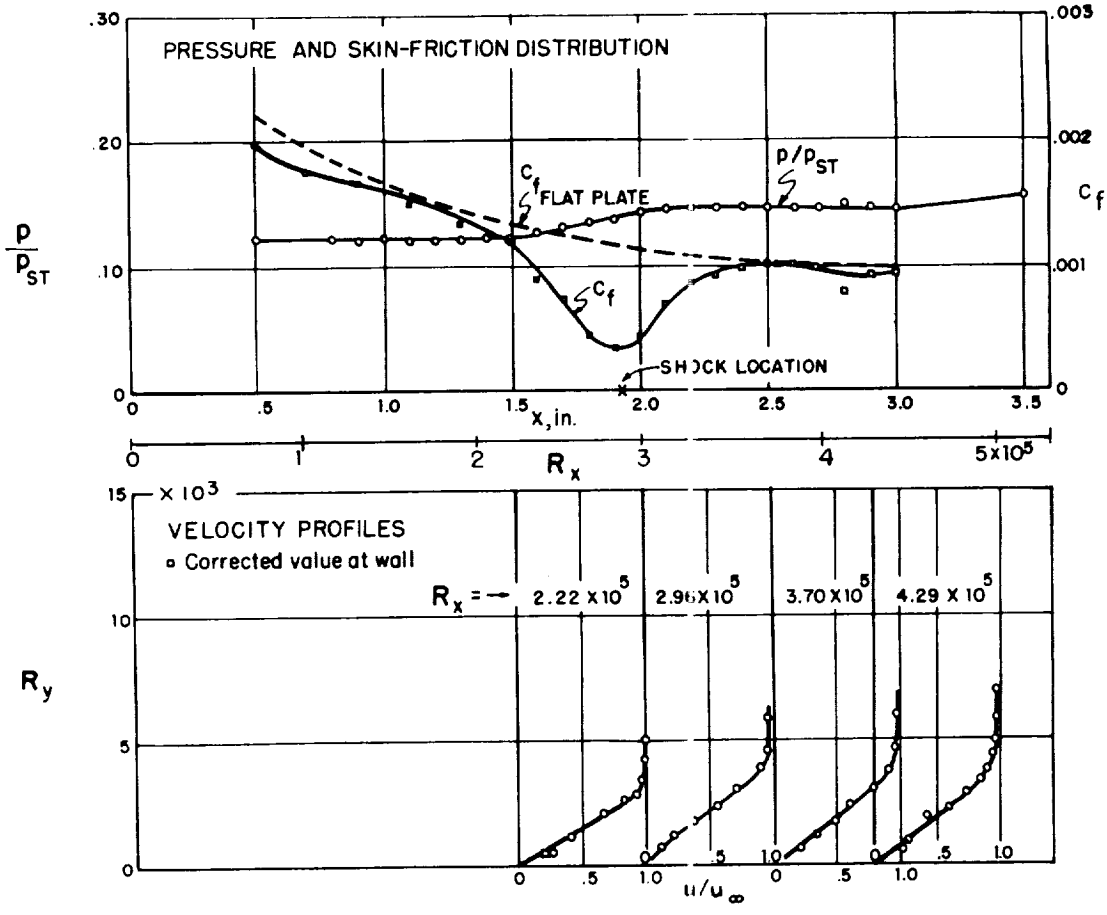

(a) $R_{shock} = 2.84 \times 10^5$; $p_2/p_0 = 1.20$.

Figure 6.- Sample pressure and wall shear distributions and velocity profiles.

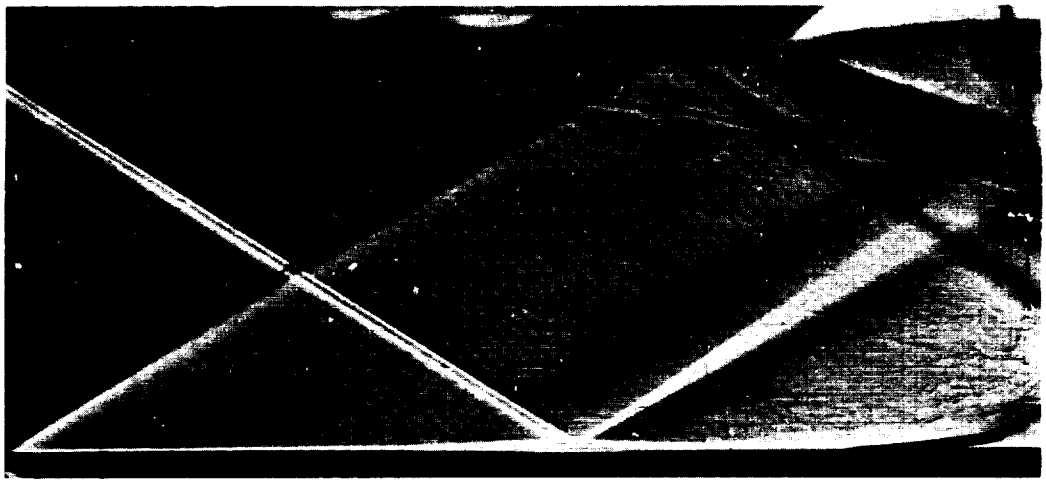

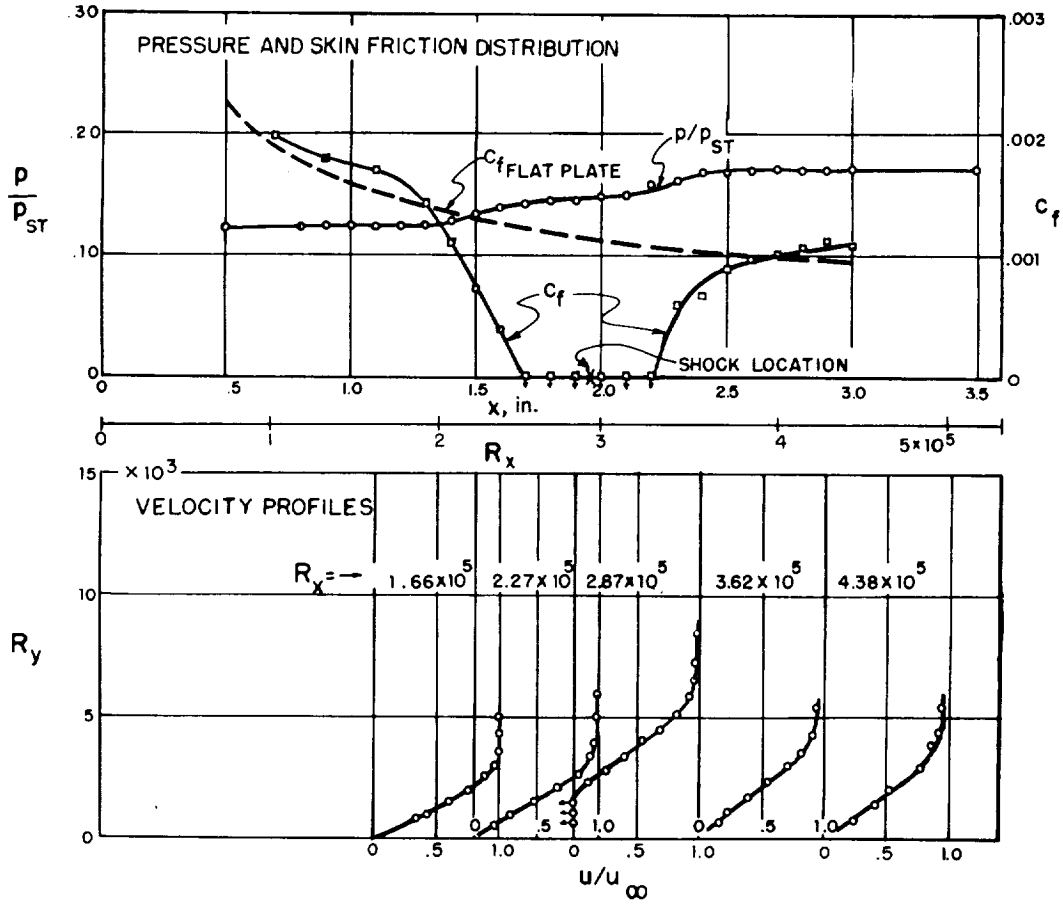

(b) $R_{shock} = 2.96 \times 10^5$; $p_f/p_o = 1.40$.

Figure 6.- Continued.

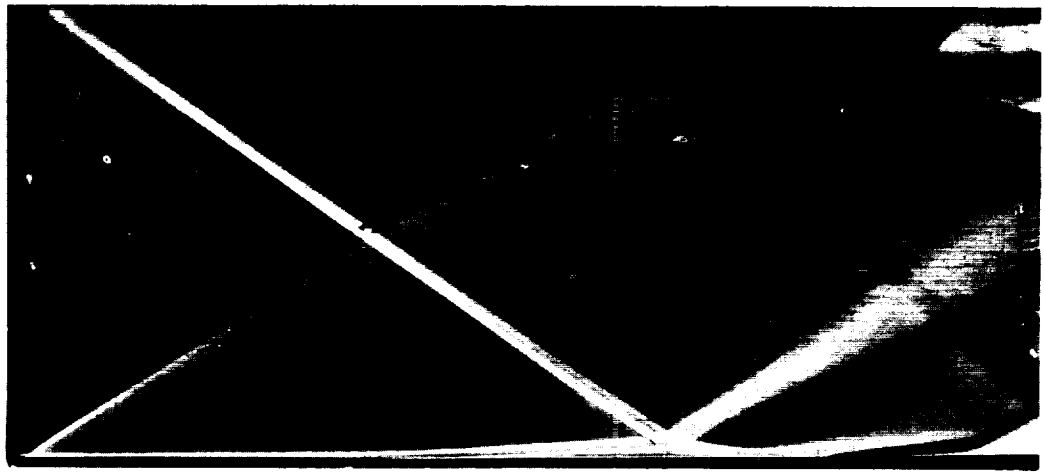

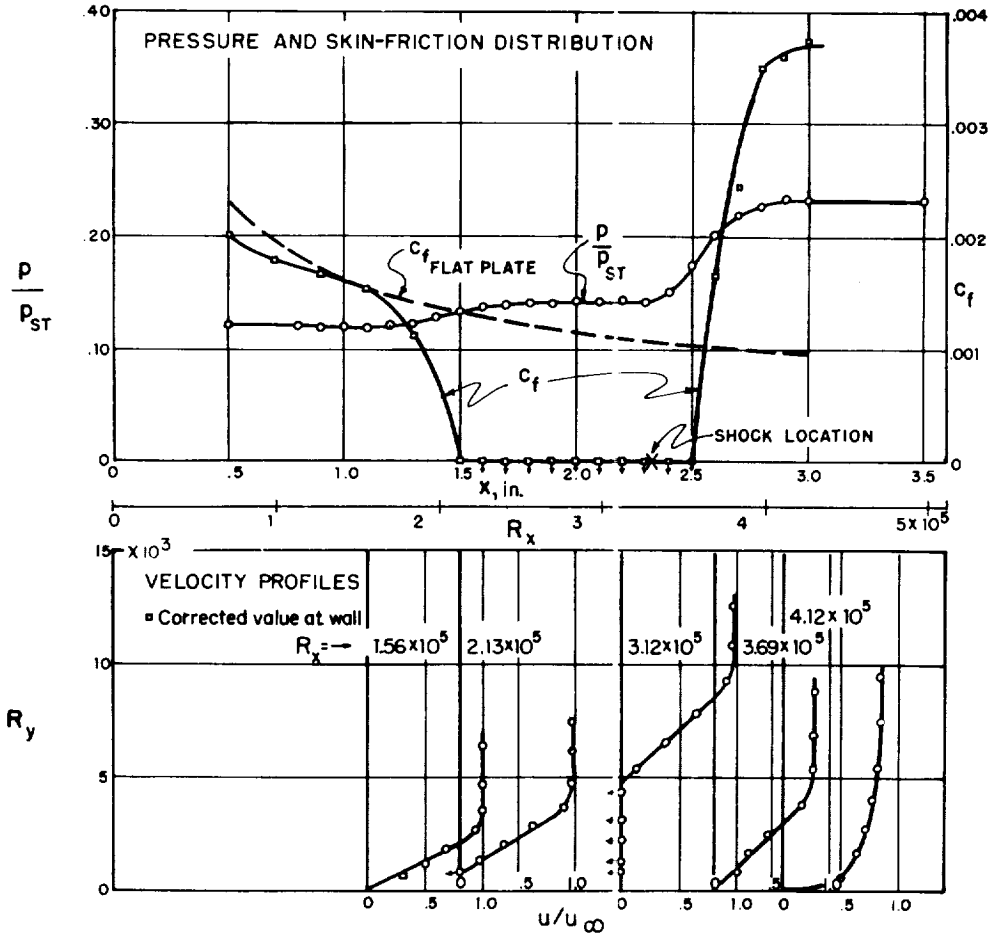

(c) $R_{shock} = 3.29 \times 10^5$; $p_f/p_o = 1.91$.

Figure 6.- Concluded.

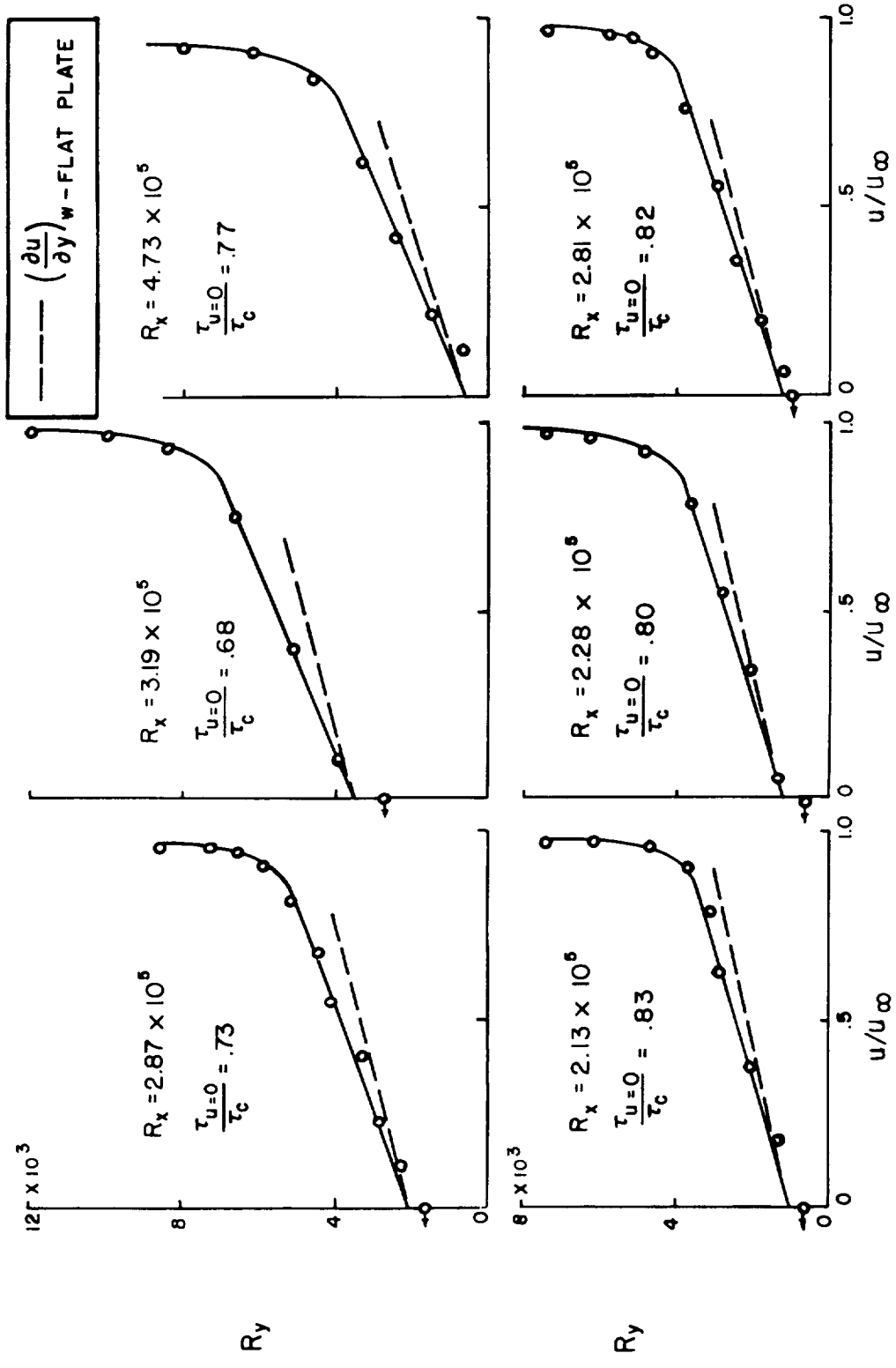

Figure 7.- Velocity profiles in separated flow.

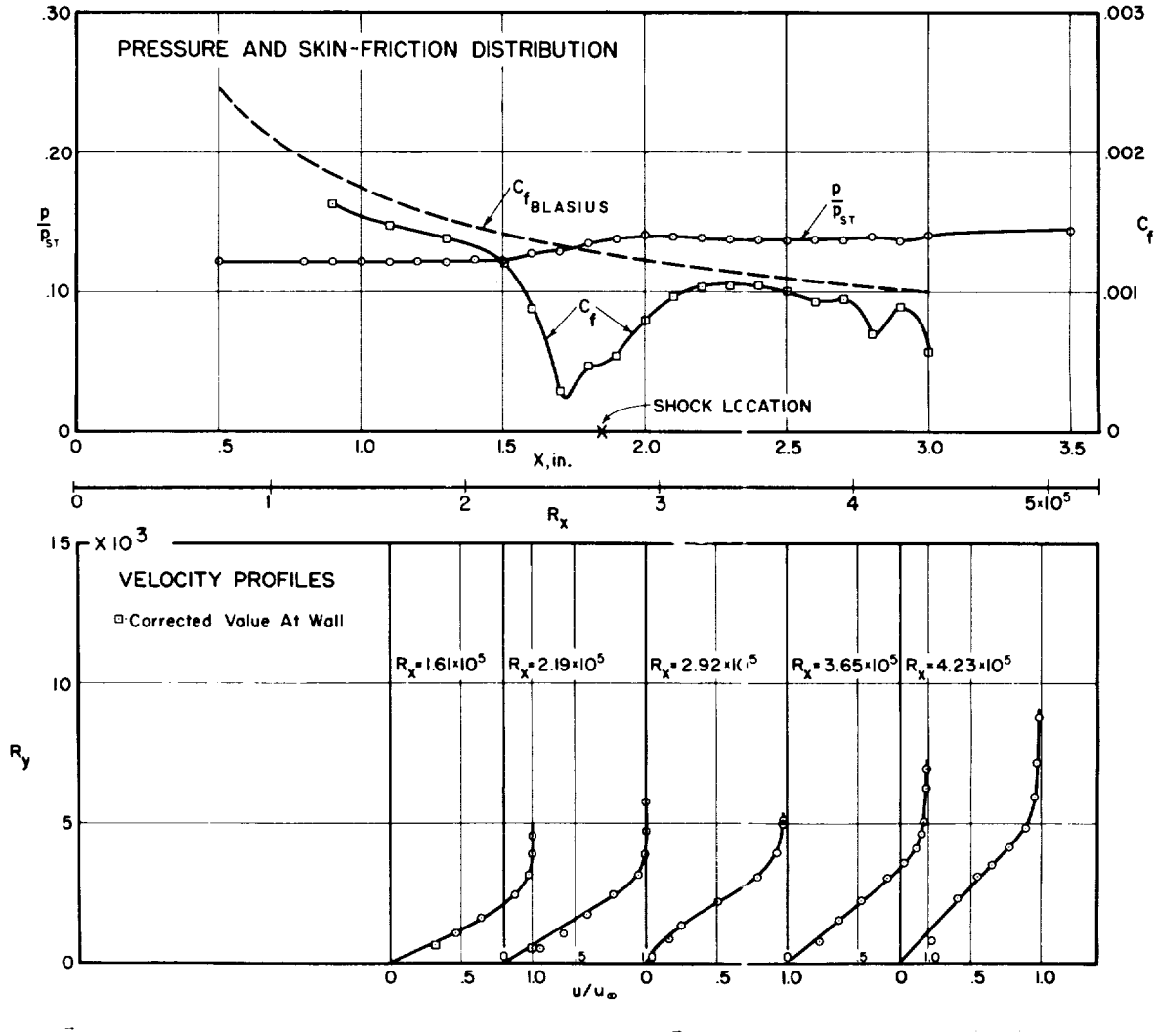

(a) $R_{shock} = 2.70 \times 10^5$; $p_f/p_0 = 1.15$.

Figure 8.- Pressure and wall shear distributions and velocity profiles.

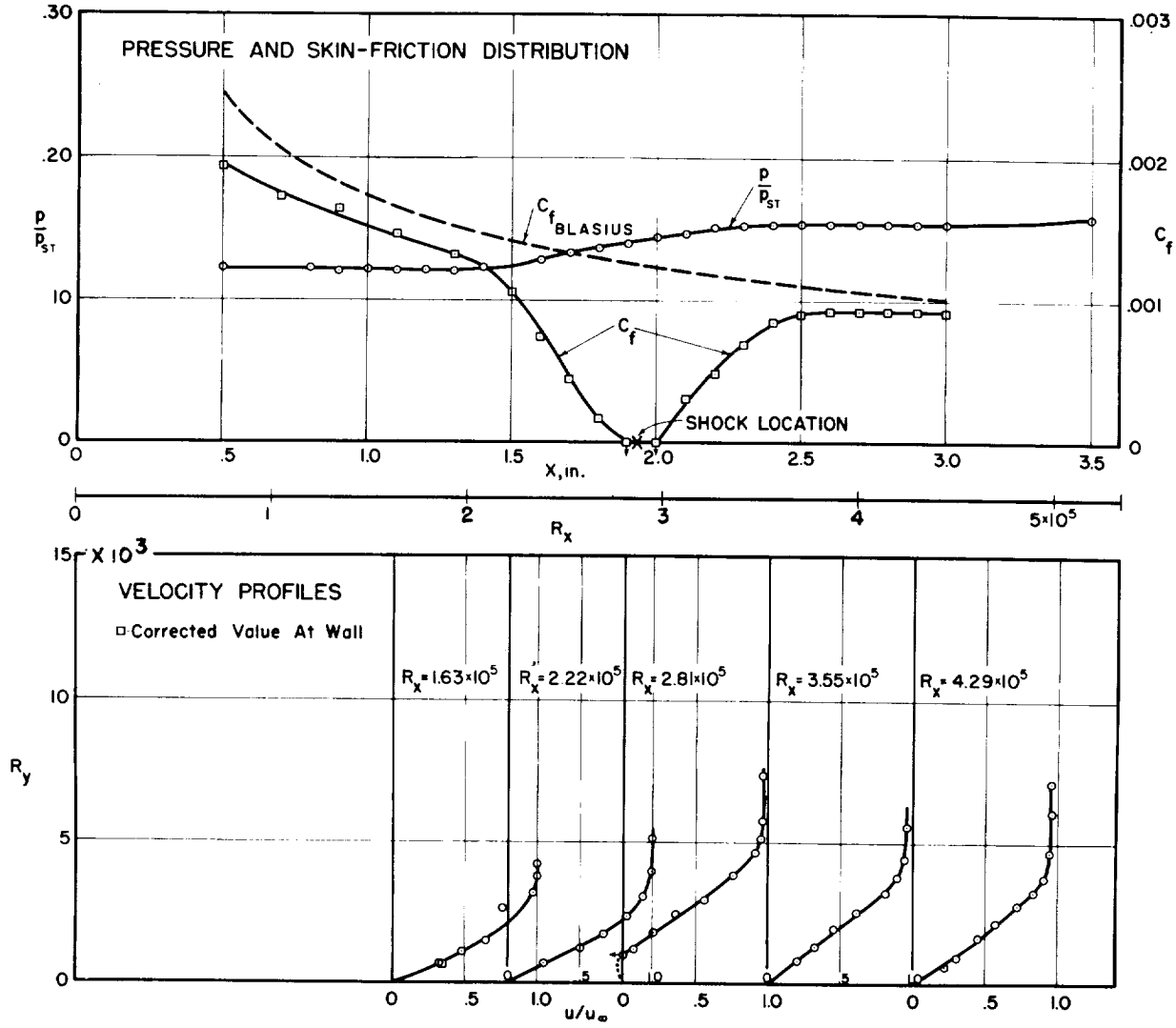

(b) $R_{shock} = 2.87 \times 10^5$; $p_f/p_o = 1.25$.

Figure 8.- Continued.

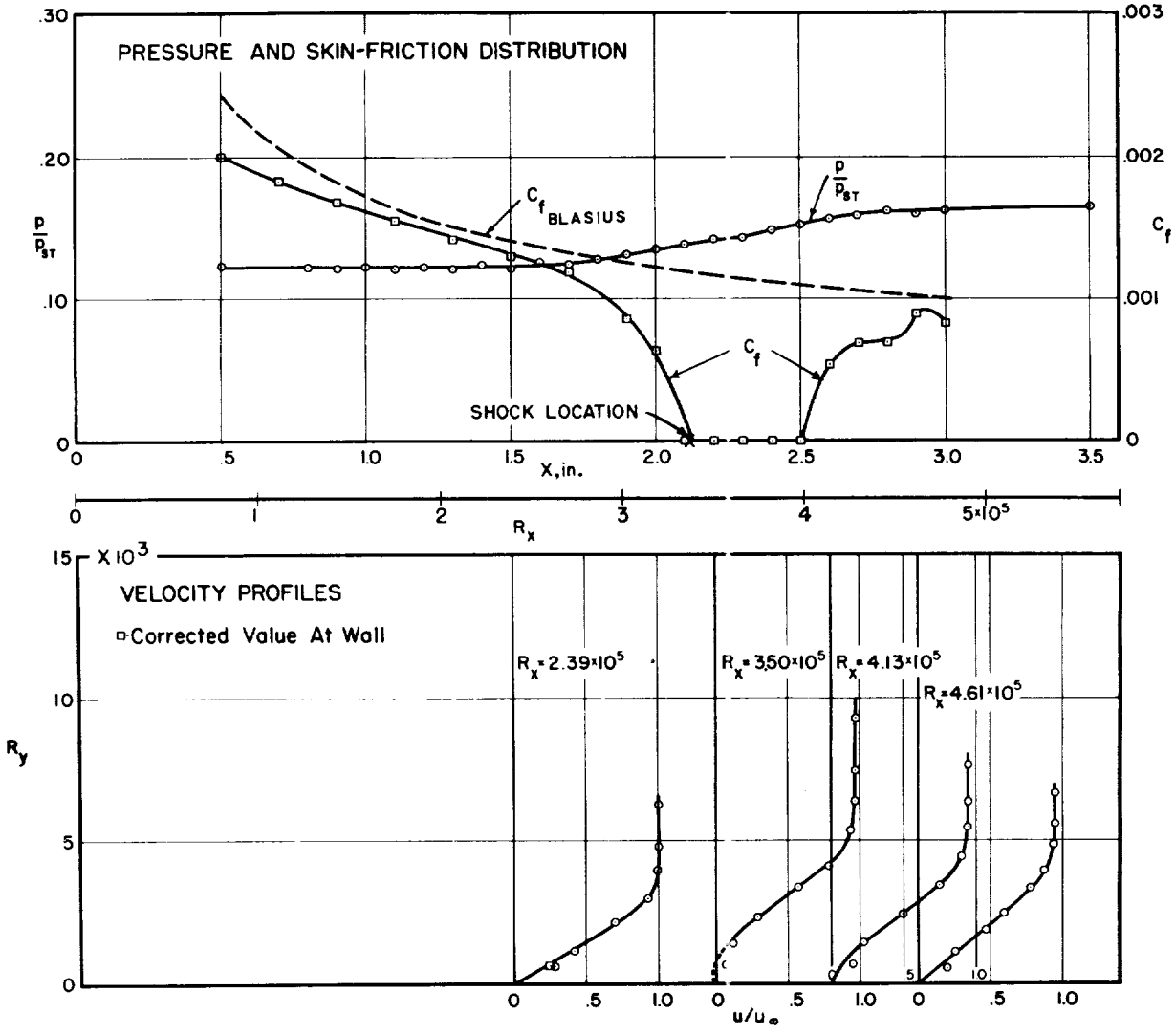

(c) $R_{shock} = 3.37 \times 10^5$; $p_f/p_o = 1.32$.

Figure 8.- Continued.

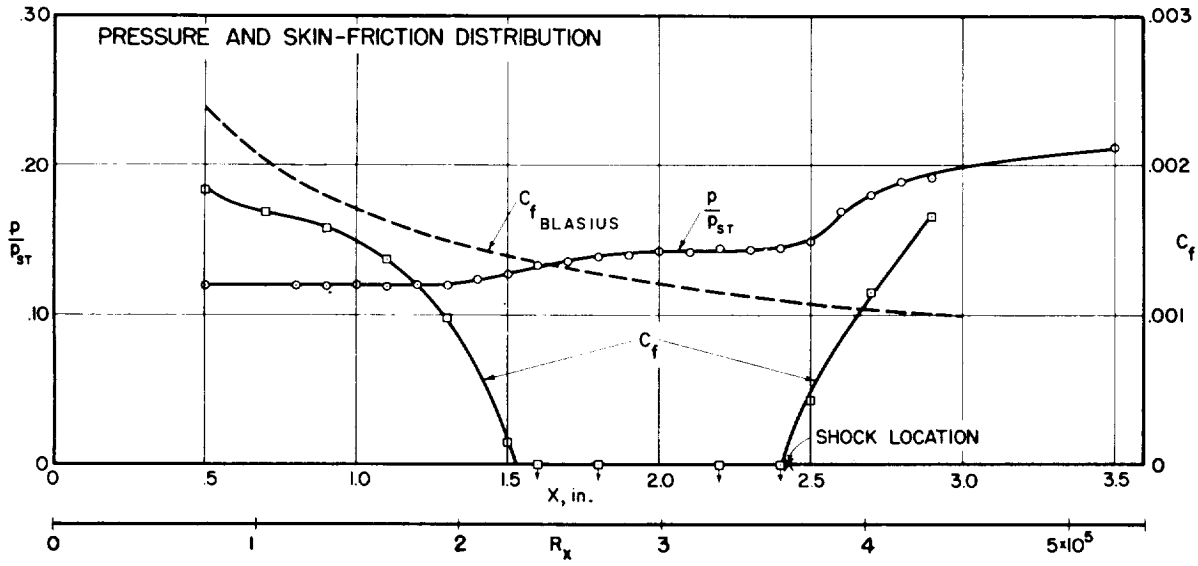

(d) $R_{shock} = 3.65 \times 10^5$; $p_f/p_o = 1.75$.

Figure 8.- Continued.

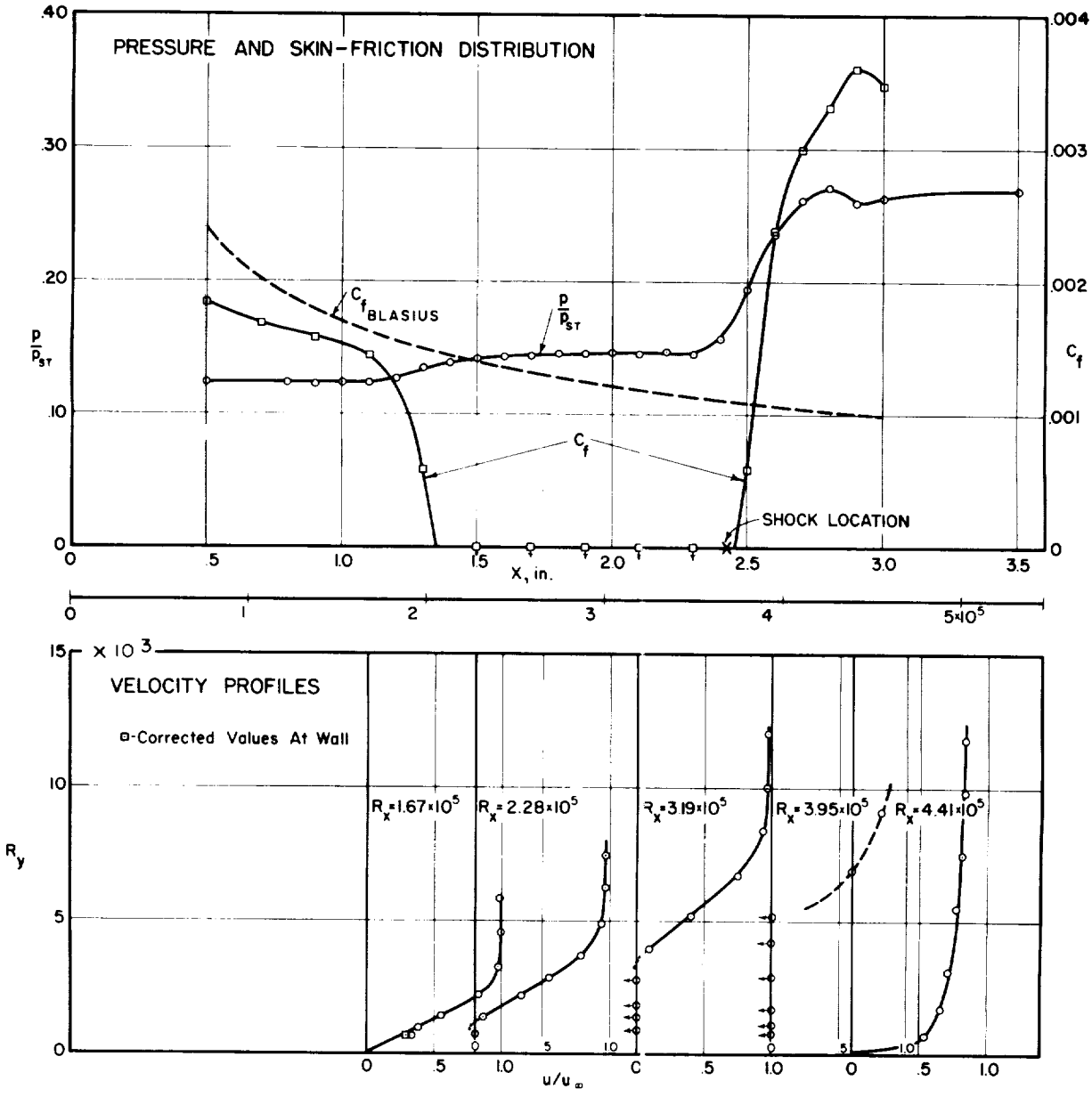

(e) $R_{shock} = 3.69 \times 10^5$; $p_f/p_o = 2.16$.

Figure 8.- Continued.

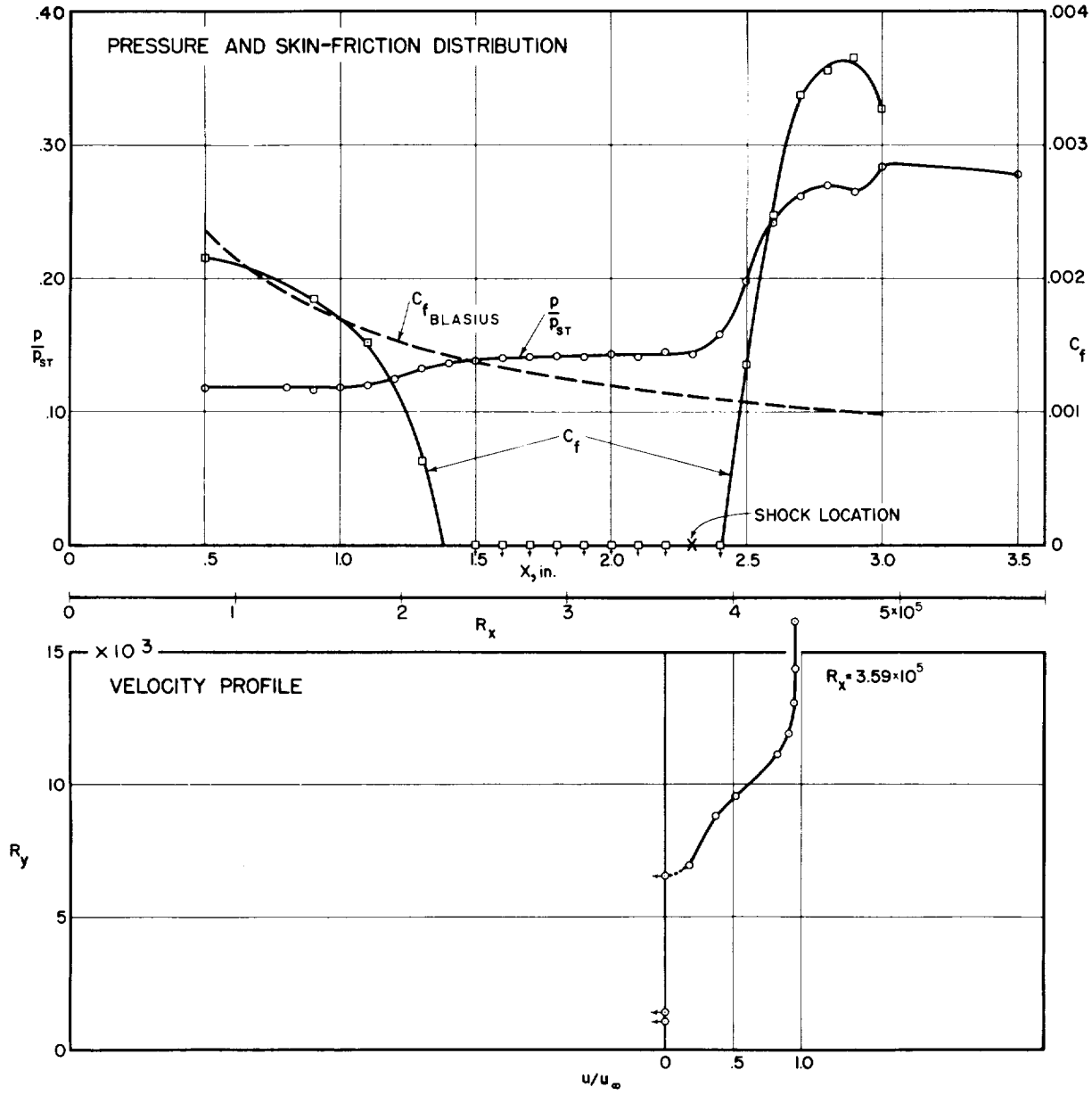

(f) $R_{shock} = 3.74 \times 10^5$; $p_f/p_o = 2.40$.

Figure 8.- Continued.

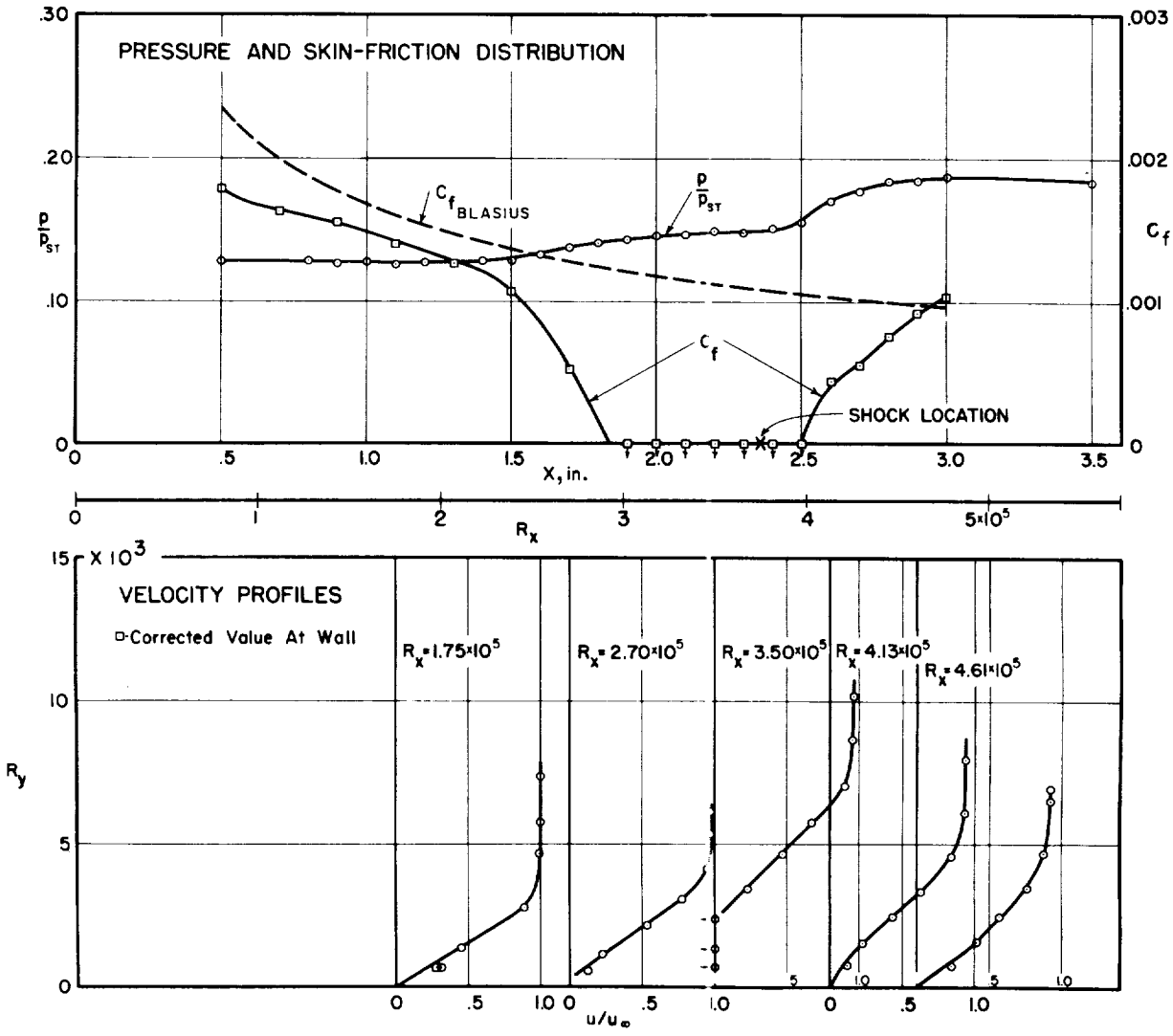

(g) $R_{shock} = 3.75 \times 10^5$; $p_f/p_o = 1.46$.

Figure 8.- Continued.

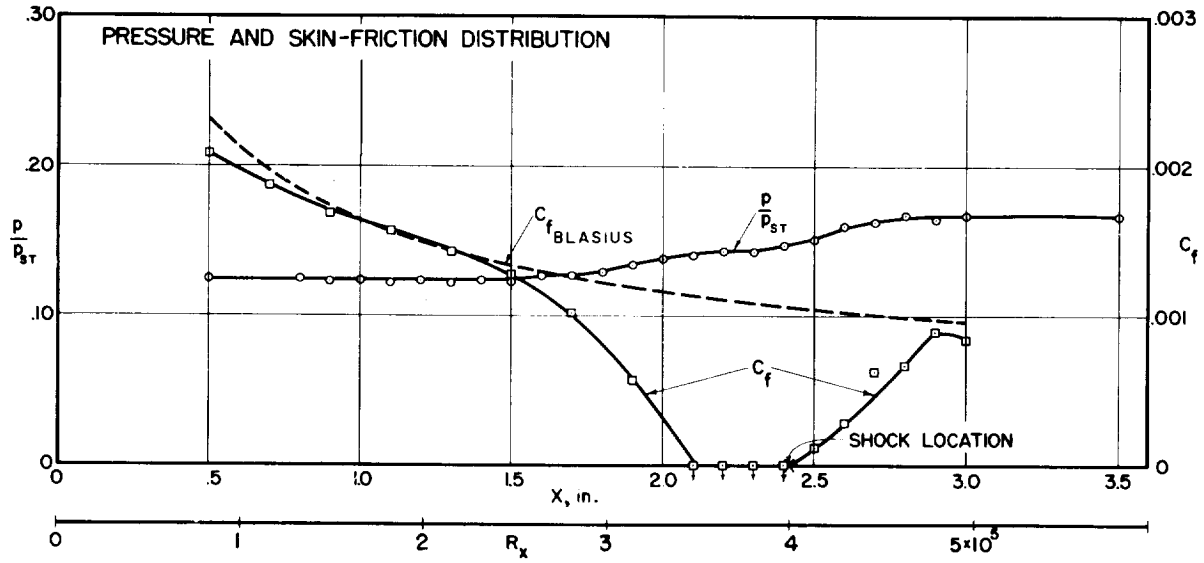

(h) $R_{shock} = 3.96 \times 10^5$; $p_f/p_o = 1.35$.

Figure 8.- Continued.

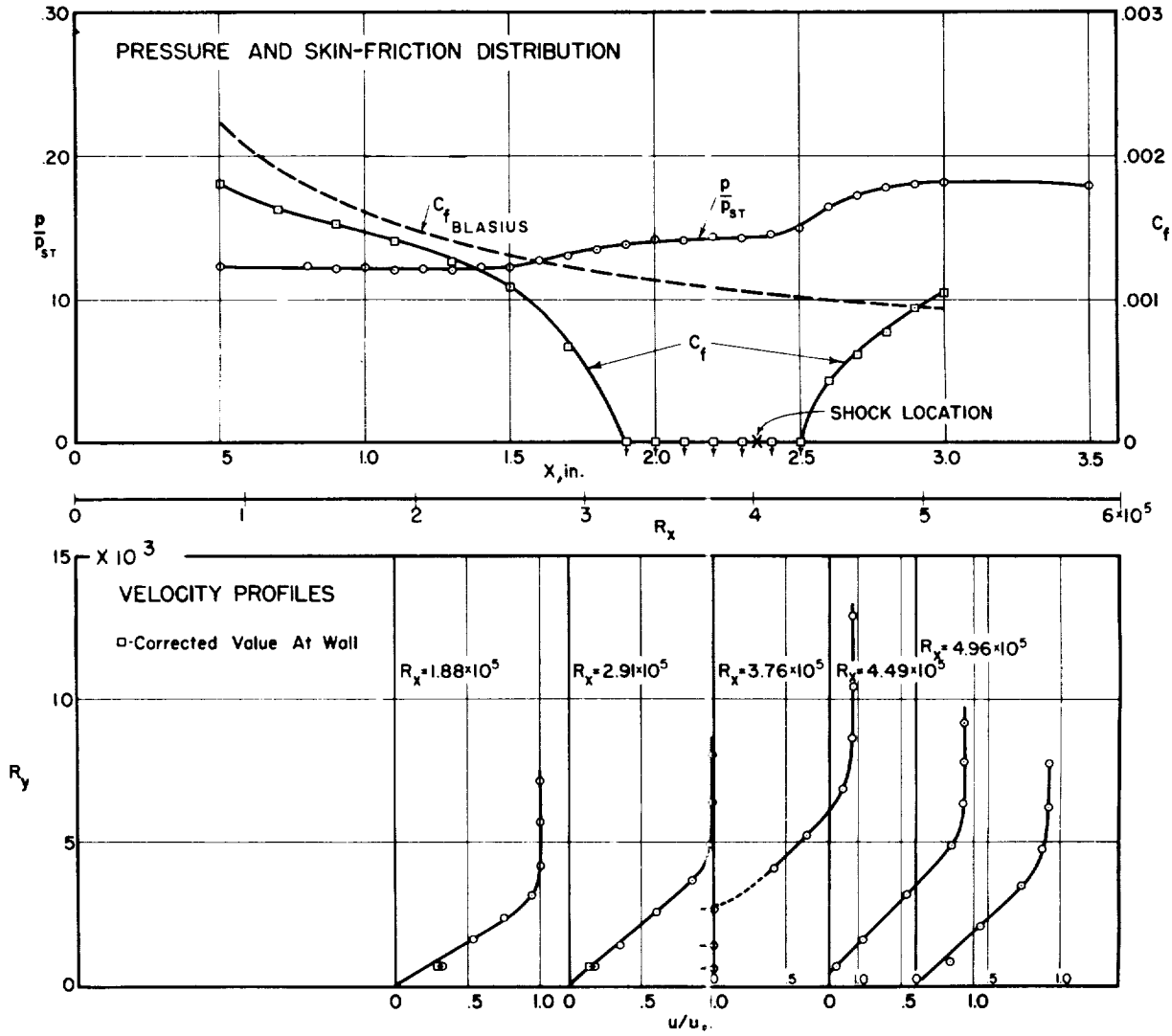

(i) $R_{shock} = 4.02 \times 10^5$; $p_f / p_o = 1.47$.

Figure 8.- Continued.

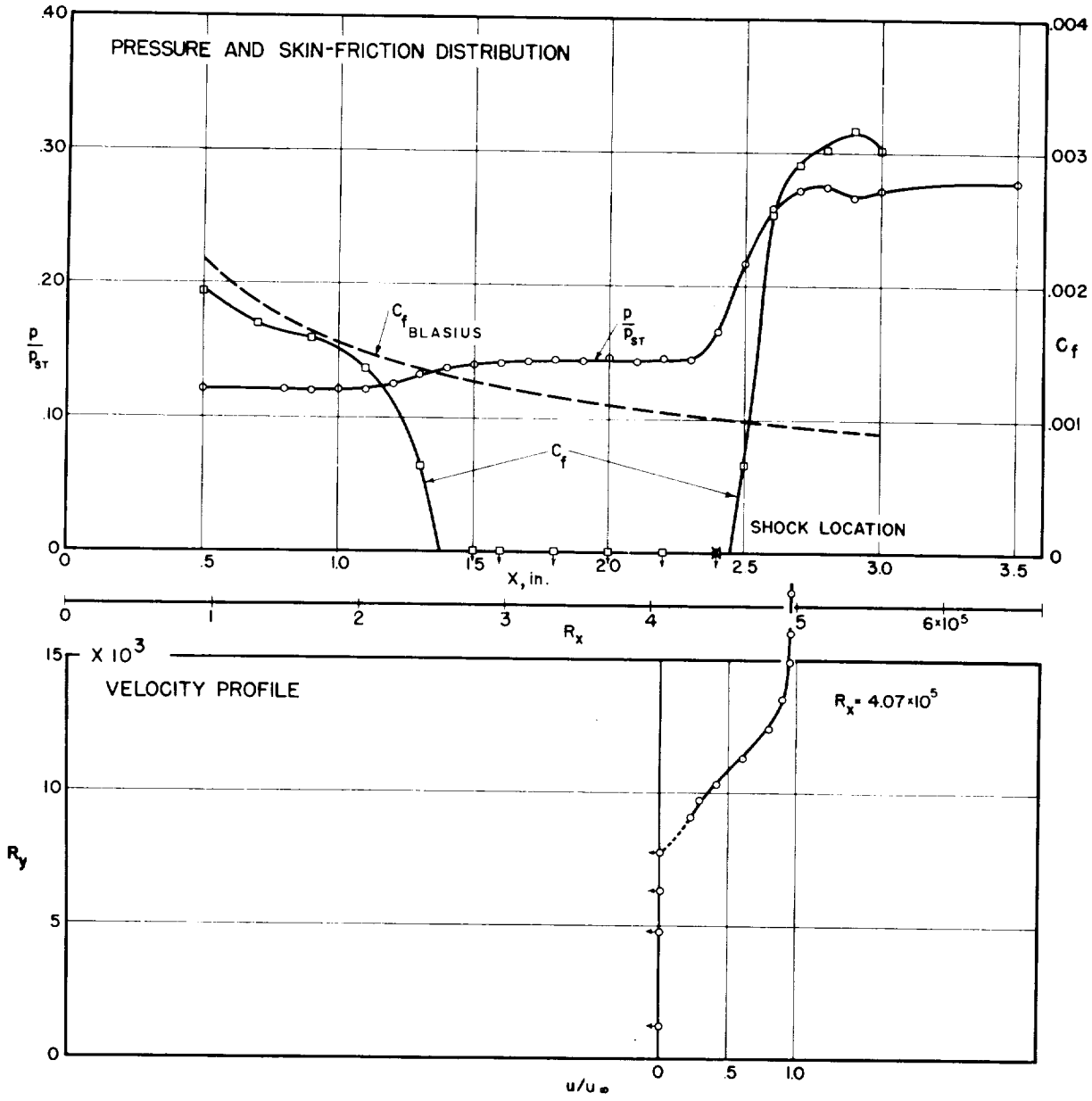

(j) $R_{shock} = 4.44 \times 10^5$; $p_f/p_o = 2.28$.

Figure 8.- Concluded.

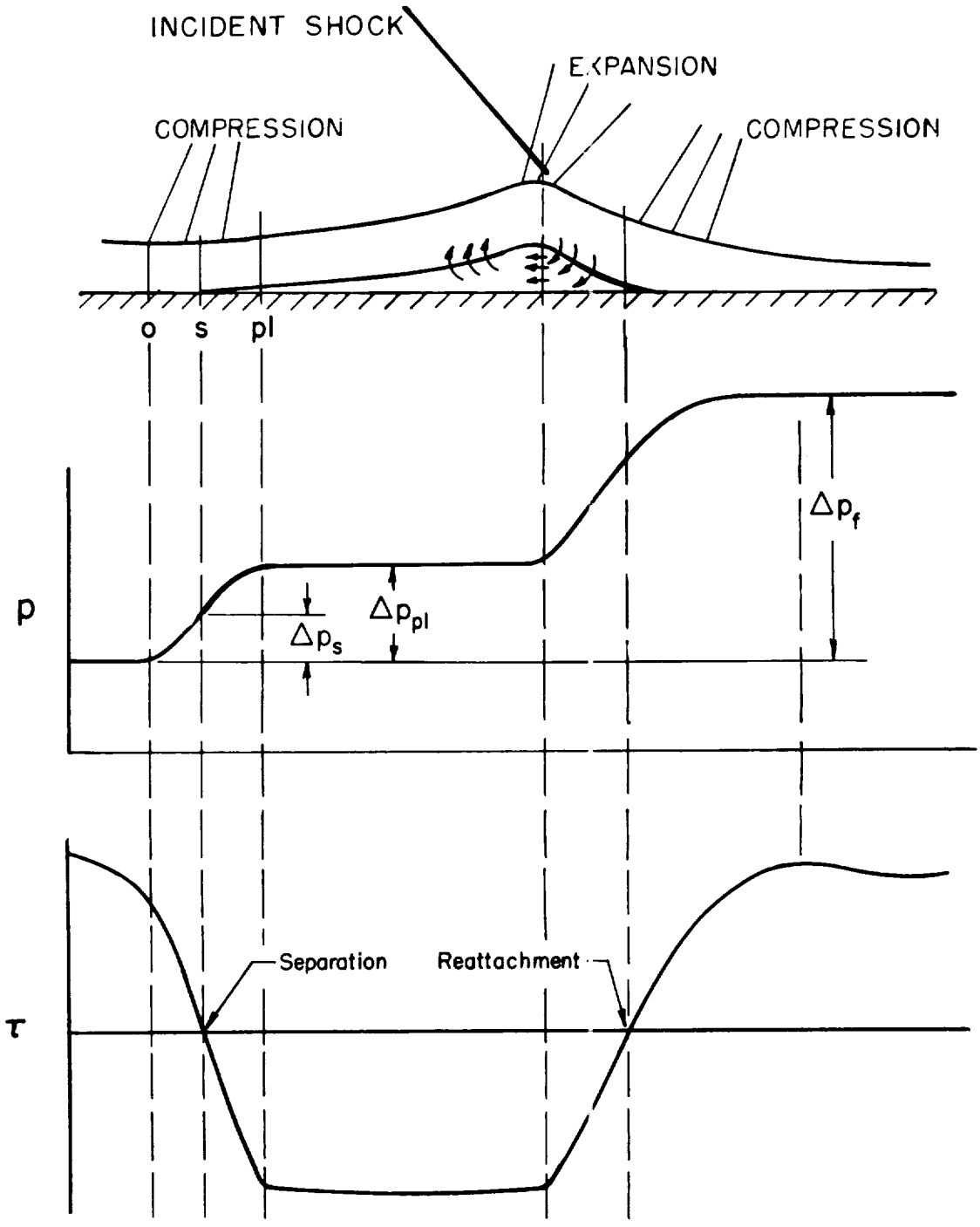

Figure 9.- Sketch of flow pattern with separated region.

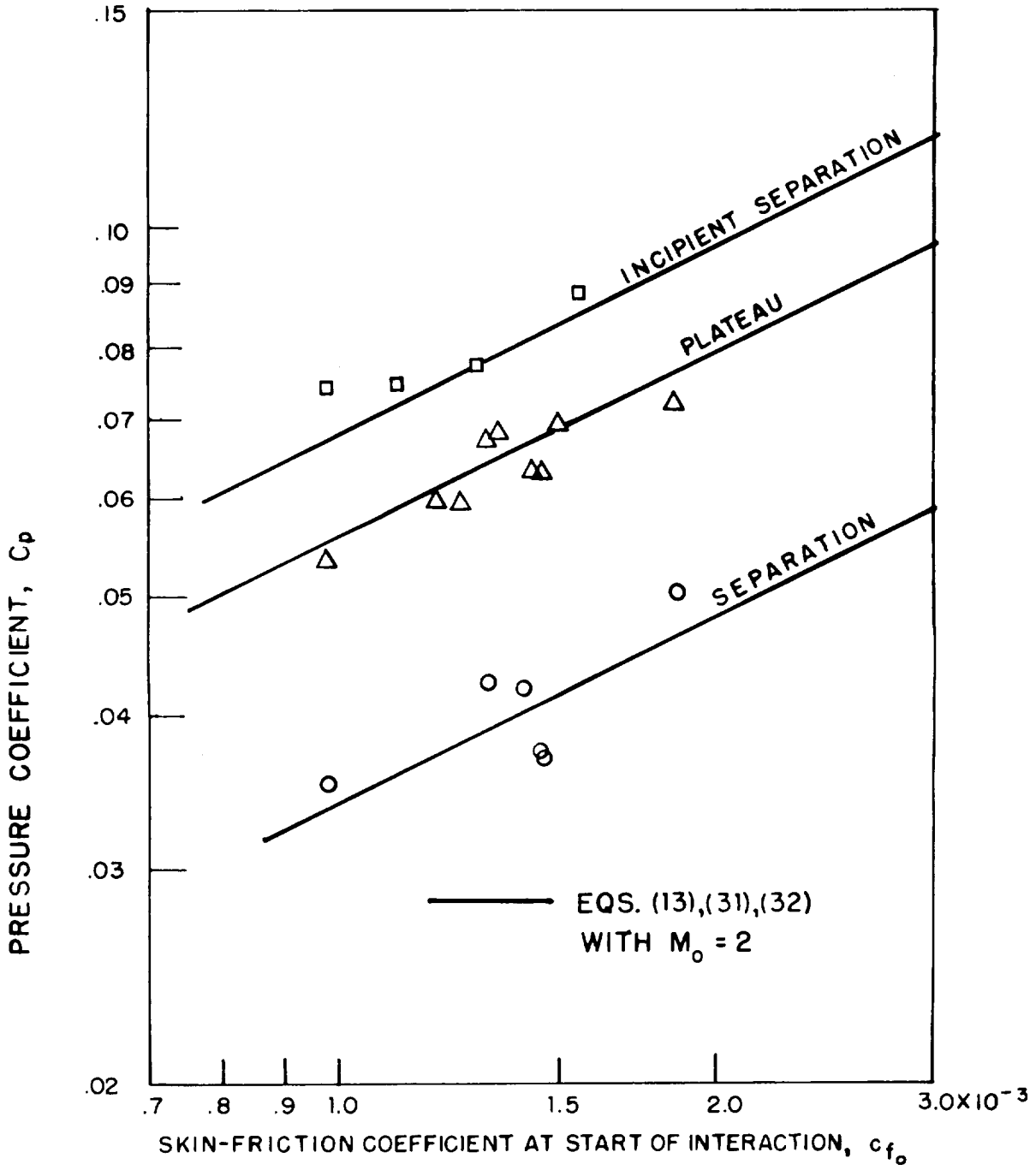

Figure 10.- Separation, plateau, and incipient separation pressure coefficients.

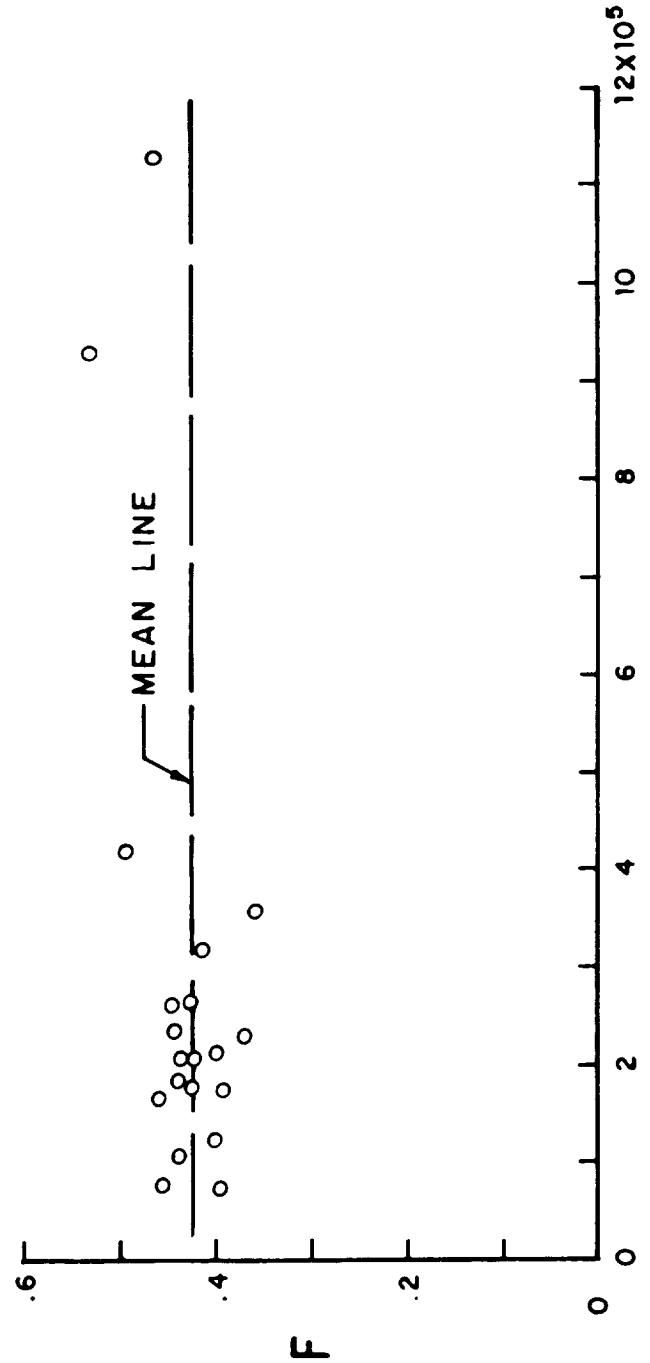

Figure 11.- Test of modified Pohlhausen-Gruschwitz separation parameter.

$$F = \frac{\left(1 + \frac{\gamma - 1}{2} r M_o^2\right)\left(x \frac{dC_p}{dx}\right)_s}{0.713} ; \quad F_{theory} = 1.$$

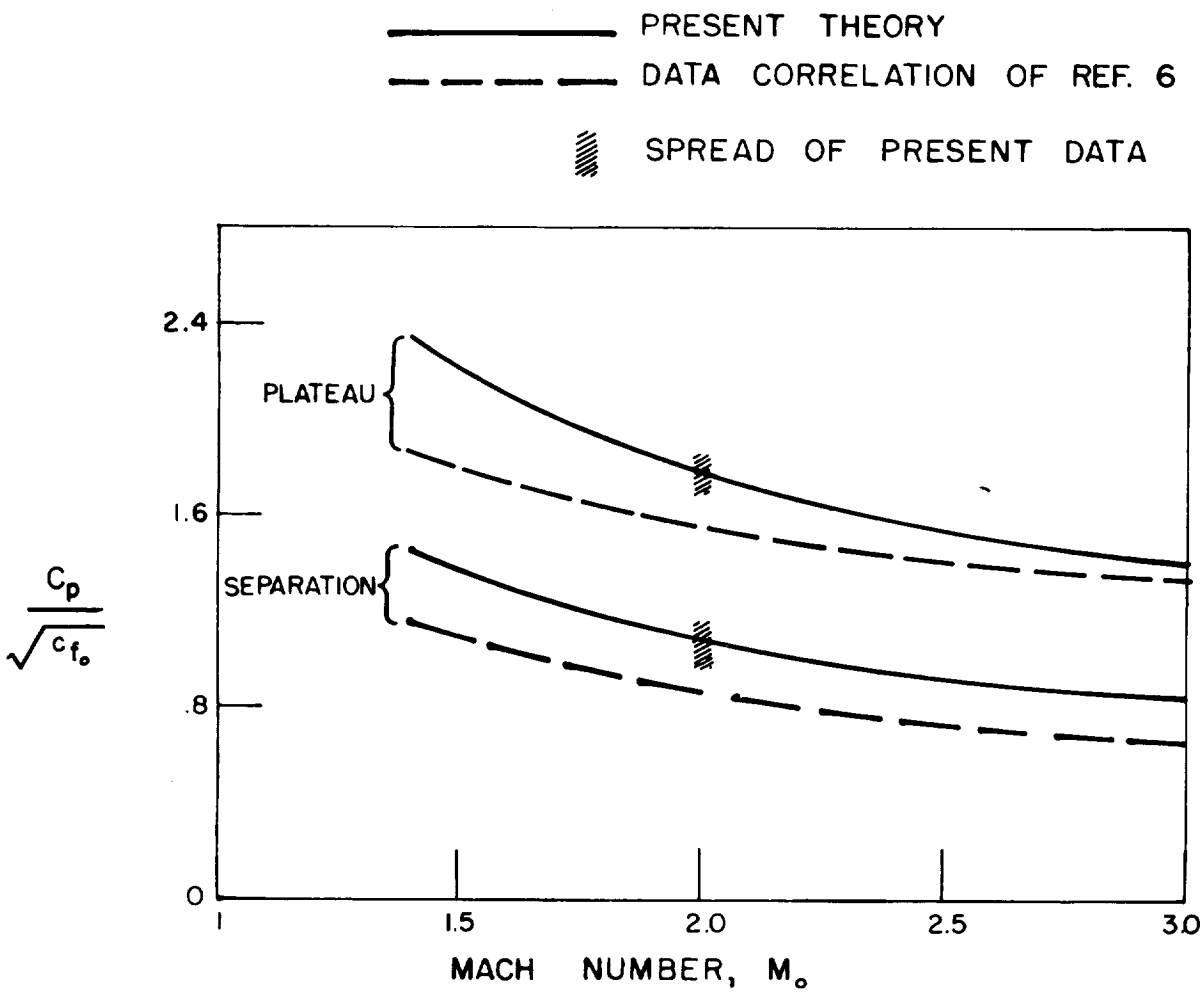

Figure 12.- Variation of separation and plateau pressure coefficients with Mach number.

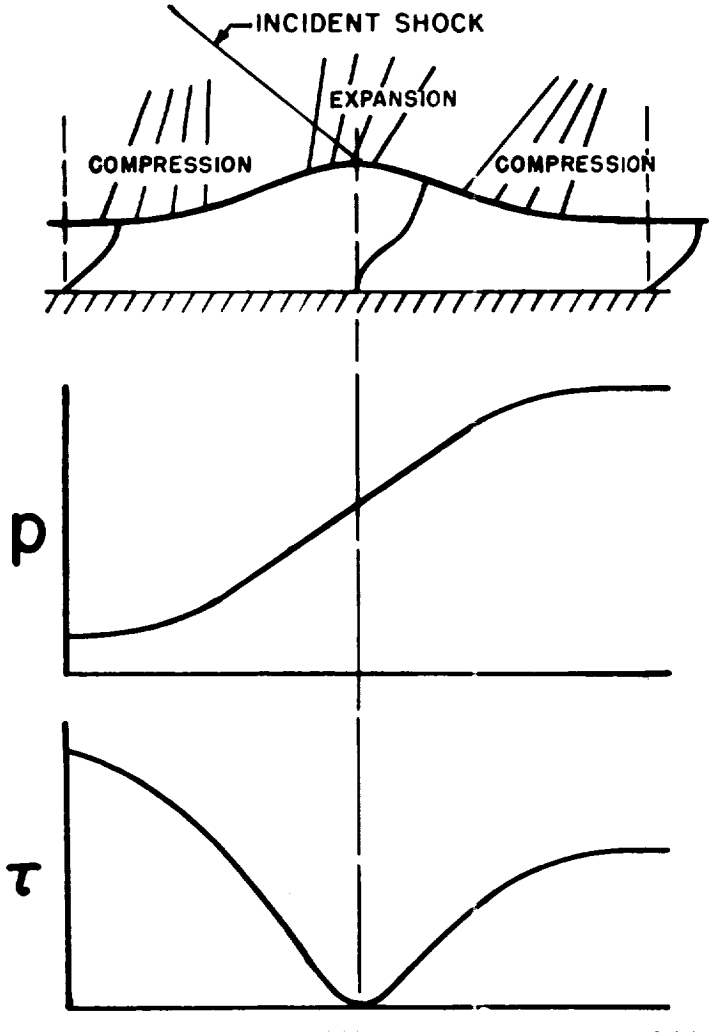

Figure 13.- Sketch of flow pattern at incipient separation.

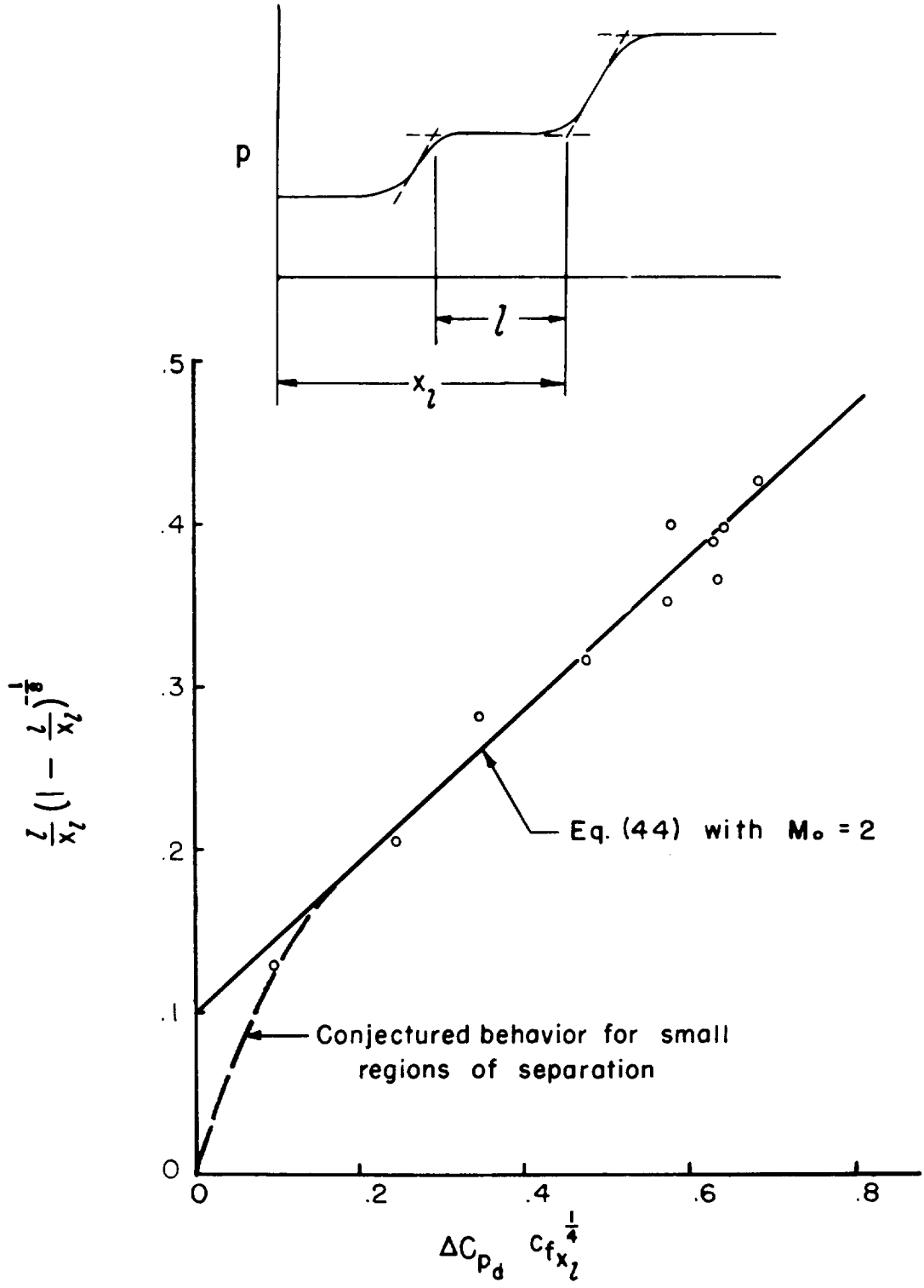

Figure 14.- Length of separation region.